bioRxiv preprint doi: https://doi.org/10.1101/153569; this version posted June 23, 2017. The copyright holder for this preprint (which was not certified by peer review) is the author/funder. All rights reserved. No reuse allowed without permission.

Dynamic balance between vesicle transport and microtubule growth enables neurite growth

Arjun Singh Yadaw, Mustafa Siddiq, Vera Rabinovich, Ravi Iyengar and Jens Hansen

Department of Pharmacological Sciences and Systems Biology Center New York, Icahn School of Medicine at Mount Sinai, New York , NY

Address correspondence to

Ravi Iyengar

Dept of Pharmacological Sciences, Box 1215

1425 Madison Rm 12-70

New York NY 10029

Ravi.iyengar@mssm.edu

bioRxiv preprint doi: https://doi.org/10.1101/153569; this version posted June 23, 2017. The copyright holder for this preprint (which was not certified by peer review) is the author/funder. All rights reserved. No reuse allowed without permission.

Abstract

Whole cell responses are complex because they involve many subcellular processes (SCPs) that need to function in a coordinated manner. Detailed understanding of how different SCPs function in a coordinated manner to produce an integrated whole cell response requires mathematical models that capture the dynamics of the individual SCPs as well as the interrelationship between the dynamics of multiple SCPs. We studied neurite outgrowth the initial process by which neurons develop axons and dendrites to understand how balance between subcellular processes is essential for the growth of neurite at experimentally observed rates. Neurite outgrowth involves two types of SCPs: membrane vesicle production/transport/fusion at the growing tip that adds membrane to the growth cone and neurite shaft, and microtubule growth and stabilization that regulates extension of the neurite shaft. Each type of SCP is composed of multiple lower level SCPs. We developed multicompartment ordinary differential equation based models to simulate how coordinated activity of these types of SCPs leads to neurite outgrowth. We utilized imaging experiments of primary cortical neurons to obtain velocities of neurite outgrowth and used these growth velocities as overall constraints with the starting postulate that the two types of SCPs involved in neurite outgrowth need to be in balance to produce a steady velocity of neurite outgrowth. We expanded previously published models of vesicle transport and microtubule growth, using experimental data from the literature to model in depth the various SCPs in each type and how they interacted. We developed analytical solutions that allowed us to calculate the relative relationships between different SCPs in a type that is needed to achieve overall balance between microtubule growth and membrane increase at the growth cone. Our models show that multiple loci within each type of SCPs are involved in obtaining balance between the two types for a specified velocity of neurite outgrowth. Parameter variation exercises allowed us to define the limits of variation within lower SCPs within a type that can be tolerated to maintain growth velocities. We conclude that as multiple SCPs come together to produce a dynamic whole cell response there is an identifiable hierarchy wherein there are redundancies at lower level SCPs, but critical quantitative interdependencies at the higher levels.

bioRxiv preprint doi: https://doi.org/10.1101/153569; this version posted June 23, 2017. The copyright holder for this preprint (which was not certified by peer review) is the author/funder. All rights reserved. No reuse allowed without permission.

Introduction

Whole cell responses that involve, both morphological and physiological changes, are complex because they can engage many subcellular processes (SCPs). Such coordinated changes often lead to change in cell state, such as moving to a more or less differentiated phenotype. Detailed understanding of how different SCPs collaborate to produce an integrated whole cell response requires both experiments, and mathematical models that capture the dynamics of the individual SCPs as well as the interrelationship between the dynamics of multiple SCPs. Neurite outgrowth is an early event that changes state of neurons (Arimura and Kaibuchi, 2007). This change in cell state allows neurons to mature by developing axons and dendritic trees that connect to other neurons and become electrically active. Many mathematical models of neurite outgrowth have been developed (Kiddie et al., 2005; Wissner-Gross et al., 2011) and these models have provided valuable insights into how complex biological processes can be modeled at various levels of description. Often these models abstract the details of the underlying mechanisms and consequently it is difficult to decipher how the balance between the various SCPs is achieved to enable whole cell responses. Some studies have focused on specific facets of the neurite outgrowth process such the role of signaling and regulatory motifs in determining how neurites get to be selected to become axons (Fivaz et al., 2008). Such models are useful in understanding regulation of complex cellular responses.

To understand how whole cell responses occur, it is necessary to delineate the quantitative balance between the dynamics of the SCPs. In the case of neurite outgrowth, two types of SCPs, membrane vesicle production/transport/fusion at the growing tip, and microtubule growth and stabilization need to be in balance to achieve neurite growth. Tsaneva-Atanasova et al (Tsaneva-Atanasova et al., 2009) developed a model that studies interaction between microtubules and membrane vesicles in regulating network outgrowth. The framework of this model serves as a useful starting point for more extensive models where we can consider how a group of distinct but related SCPs such as vesicle budding, vesicle transport and vesicle fusion along with a second group of SCPs that involves microtubule nucleation, microtubule growth and conversion of active to stable microtubules interact to enable the growth of neurites. Such detailed models could serve as basis for determining the relationship between the kinetic parameters and changes in levels or activities of molecular components within the different SCPs could be regulated by signaling networks. To develop a detailed model of neurite outgrowth based on interactions between SCPs of different types, we constructed a multi compartment ordinary differential equation model to extend and integrate the microtubule growth model developed by Margolin et al (Margolin et al., 2012) with the vesicle transport model by Heinrich and Rappaport (Heinrich and Rapoport, 2005) with additional details to make the overall model contemporary, taking into account experimental data that have been published since these models were published.

We have made a critical change from our previous approaches to dynamical modeling in developing this model. We had typically used a bottom up approach where individual reactions are assembled into modules that have emergent behaviors (Azeloglu et al., 2014; Bhalla and

bioRxiv preprint doi: https://doi.org/10.1101/153569; this version posted June 23, 2017. The copyright holder for this preprint (which was not certified by peer review) is the author/funder. All rights reserved. No reuse allowed without permission.

Iyengar, 1999). In contrast the approach we use here can be called top down as we made a starting postulate that the two types of SCPs involved in neurite outgrowth need to be in balance to produce a steady velocity of neurite outgrowth. The two types of SCPs are, 1) the membrane vesicle production/movement/fusion and expansion of the growth cone related processes and 2) the microtubule growth and elongation related processes. We start with experimental observations of the velocity of neurite outgrowth and used numerical simulations and comparison to experimental results to determine the loci that could be used to control the balance between the two types of SCPs such that we could obtain experimentally observed growth velocities. Our models show that multiple loci within each type of SCPs are involved in obtaining balance between the two types of SCPs We used analytical solutions to map these loci through parameter variation exercises to understand how different groups of SCPs are balanced within each type and between types to mount a whole cell response.

bioRxiv preprint doi: https://doi.org/10.1101/153569; this version posted June 23, 2017. The copyright holder for this preprint (which was not certified by peer review) is the author/funder. All rights reserved. No reuse allowed without permission.

Results

MODEL

The computational model we describe here consists of two parts representing the two types of SCPs involved. The first part consists of membrane vesicle production/budding/transport and fusion and the second part consists of microtubule assembly/growth/stabilization.

Membrane Vesicle Related SCPs

Our vesicle model for membrane delivery to the growing neurite tip is based on a dynamical model of bidirectional membrane and membrane protein transport between the endoplasmic reticulum and the cis-Golgi (Heinrich and Rapoport, 2005). In our model the two organelles are the Trans-Golgi-Network (TGN) and the Growth Cone (GC) of the neurite (Figure 1A). Newly synthesized membrane is synthesized in the cell body (Gracias et al., 2014; Wang et al., 2011), added to the TGN (Reaction 1 in Table 1 and Figure 1A) and transported via vesicular transport to the neurite tip to enable neurite shaft growth after fusion with the growth cone (Nakazawa et al., 2012; Pfenninger, 2009; Wang et al., 2011). Between the TGN and GC are 3 different cytoplasmic compartments: the cell body (CB) cytoplasm, the Microtubule Transport Compartment (MTC) that extends over the whole neurite shaft and the growth cone (GC) cytoplasm. All three compartments contain microtubule bundles allowing microtubule based vesicle transport from one compartment into the other. Anterograde vesicles bud from the TGN into the CB cytoplasm, move through the MTC into the GC cytoplasm and fuse with the GC membrane. Retrograde vesicles are endocytosed from the growth cone membrane and move through the three cytoplasmic compartments in the opposite direction to finally fuse with the TGN.

Budding at either the TGN or GC is mediated by site-specific budding machineries (McNiven and Thompson, 2006). Endocytosis, for example, is mediated by specialized mechanisms such as clathrin- or caveolin-mediated endocytosis (Godlee and Kaksonen, 2013; Lajoie and Nabi, 2007; Mettlen and Danuser, 2014), while different mechanisms are involved in the budding of vesicles from the TGN (Kienzle and von Blume, 2014; Kim, 2016). Such site-specificity is achieved in the Heinrich and Rappaport model by two different coat proteins, coat B and coat A, that are recruited to the membrane of the donor-organelle by two different recruitment factors, recruitment factor 1 and recruitment factor 2 (Reaction 2 in Table 1 and Figure 1). Recruitment factor 1 recruits coat protein B to the membrane of the organelle to initiate the budding process, recruitment factor 2 recruits coat protein A. Site-specificity of the recruitment process is achieved by an accumulation of recruitment factor 1 at the TGN and recruitment factor 2 at the GC. We additionally introduce site-specificity of the coat proteins by assuming that coat protein B mainly resides in the CB cytoplasm, while coat protein A in the GC cytoplasm. This assumption is implemented by site-specific budding rates (Reaction 2 in Table 1).

bioRxiv preprint doi: https://doi.org/10.1101/153569; this version posted June 23, 2017. The copyright holder for this preprint (which was not certified by peer review) is the author/funder. All rights reserved. No reuse allowed without permission.

During the budding process the coat proteins incorporate membrane proteins from the donor organelle into the budding vesicles (Brodsky, 2012; Kienzle and von Blume, 2014; McNiven and Thompson, 2006; Sochacki et al., 2017), a step needed for completion of the budding process (Ehrlich et al., 2004). The coat proteins have different affinities towards the membrane proteins (reactions 3-5 in Table 1). Following the model of Heinrich and Rapaport we postulate that coat protein B has a high affinity for those membrane proteins that are involved in anterograde vesicle movements, e.g. in anterograde vesicle movement along the microtubules or vesicle fusion with the growth cone, while coat protein A has a high affinity for those membrane proteins that are involved in retrograde vesicle movement (Table 2). This ensures the budding of vesicles with the right set of membrane proteins, but also causes an accumulation of membrane proteins involved in anterograde transport at the GC and of membrane proteins involved in retrograde transport at the TGN. To ensure availability of the membrane proteins for the next set of budding vesicles, they need to be back transported. Thus, coat protein A also binds membrane proteins that are involved in anterograde transport and coat protein B membrane proteins that are involved in retrograde transport, though with a lower affinity (Table 2).

In contrast to the original Henrich and Rappaport model we do not allow back fusion of newly budded vesicles to the TGN or GC, but assume that they immediately move towards the GC or CB. Regulatory mechanisms that prevent the back fusion have been identified for ER budded vesicles (Lord et al., 2011). Endocytosed vesicles are transported via an actin comet tail into the cell interior (Collins et al., 2011), a mechanism that should significantly lower the chance of back fusion of these vesicles to the plasma membrane. Simultaneously, a mechanism that mediates loading of TGN-derived vesicles onto the microtubules during budding has been described in neurons (Burgo et al., 2012), that should allow the immediate forward transport of these vesicles and remove them from the TGN.

Vesicles are transported along microtubules via active motor proteins that they bind with their membrane motor protein receptors (Reactions 6-7 in Table 1A and Figure 1A). Anterograde vesicles movement along the microtubules is mediated via kinesin that is bound to kinesin receptors, retrograde vesicle movement via dynein that is bound to dynein receptors. We assume that motor protein receptors on vesicles are always occupied by motor proteins and that only vesicles that are bound to the microtubules via a motor protein are actively transported into the desired direction. The dissociation constants of motor proteins to the microtubule differ in the different compartments, implemented into our model via pre-defined fractions of bound dynein and kinesin (Table 1C). The CB cytoplasm has a very high fraction of bound kinesin molecules, resembling the observation that anterograde vesicles are loaded onto the microtubule in a Microtubule-Actin Crosslinking Factor 1 (MACF1) dependent process right after budding to assure immediate anterograde vesicle movement (Burgo et al., 2012). Kinesin competes with the microtubule associated protein tau for microtubule binding spots (Dixit et al., 2008; Ebneth et al., 1998; Hagiwara et al., 1994; LaPointe et al., 2009; Seitz et al., 2002; Vershinin et al., 2007). Multiple studies report an increasing gradient of tau from the neurite base to the GC (Black et al.,

bioRxiv preprint doi: https://doi.org/10.1101/153569; this version posted June 23, 2017. The copyright holder for this preprint (which was not certified by peer review) is the author/funder. All rights reserved. No reuse allowed without permission.

1996; Kempf et al., 1996; Mandell and Banker, 1996). We included this gradient of tau protein mediated kinesin binding inhibition into our model by decreasing the fraction of MT-bound kinesin molecules from the CB cytoplasm to the MTC and further in the GC cytoplasm (Table 4). Such an increase is also in agreement with the observation that only a few vesicles (~9%) in axons are moving forward, while the majority of vesicles only shows random diffusion based movements (Ahmed and Saif, 2014), implicating that the MTC compartment functions as a vesicle reservoir for membrane recruitment on demand. Concordantly, neurites continue growing for about 6h after disruption of the TGN, the source of newly generated membrane (Prager-Khoutorsky and Spira, 2009). No kinesin molecules are bound to the MT in the GC cytoplasm, so that all vesicles dissociate from the MT and are available for fusion with the GC membrane. The binding of dynein to the microtubules is not significantly affected by tau (Dixit et al., 2008), allowing a high fraction of MT-bound dynein in the GC cytoplasm. In contrast to kinesin, the fraction of MT-bound dynein is also high in the MTC, assuming that there is no reservoir for backward moving vesicles and that these vesicles are transported back to the TGN without any hesitation as it was observed for components of the degradative pathways such as autophagosomes (Fu et al., 2014; Maday et al., 2012). In the CB cytoplasm no dynein molecules are bound to the MT, allowing the fusion of retrograde vesicles with the TGN. To simulate active motor protein mediated vesicle transport along the microtubule we assume that once a vesicle is attached to the microtubule with at least one motor protein, it is actively transported along the microtubule with a constant velocity that does not increase with further attached motor proteins, as also proposed by others (Vershinin et al., 2007). We calculated the fraction of bound vesicles based on the fraction of bound motor proteins (reactions 6a/b and 7a/b in Table 1) and based on this the rate of vesicle movement along the microtubule into the next compartment along the microtubule track, e.g. the MTC or GC cytoplasm (Reactions 6c and 7c in Table 1).The rate of vesicle movement calculated under the steady-state assumption that all microtubule bound vesicles of one set in one compartment are uniformly distributed along the microtubules (i.e. the distance between traveling vesicles is always the same). Thus, we can estimate the frequency of vesicle arrival at the end of the compartment by reversing the traveling time, allowing the calculation of membrane flux from each compartment into its destination compartment.

We postulate that although anterograde and retrograde vesicles both contain kinesin receptors only kinesin receptors on anterograde vesicles, but not on retrograde vesicles, and are bound to active kinesin. The same assumption is made for dynein receptors, but in the opposite way. Only dynein receptors on retrograde vesicles, but not on anterograde vesicles are bound to active dynein. This constraint and simplification accounts for back transport of the appropriate receptor to the appropriate organelle, i.e. kinesin receptor to the TGN and dynein receptor to the GC membrane and is based on multiple lines of experimental data. These experiments show that backward moving vesicles contain kinesin as a passive passenger (Fu et al., 2014; Maday et al., 2012; Prevo et al., 2015) and kinesin stimulates retrograde dynein mediated transport of prion

bioRxiv preprint doi: https://doi.org/10.1101/153569; this version posted June 23, 2017. The copyright holder for this preprint (which was not certified by peer review) is the author/funder. All rights reserved. No reuse allowed without permission.

protein vesicles (Encalada et al., 2011). Dynein is transported to the growth cone via direct interaction with kinesin (Twelvetrees et al., 2016) and is highly concentrated at the GC. Such a dynein gradient suggests that only dynein receptors at the GC, but not at the CB bind dynein.

Vesicle fusion with GC membrane is mediated via SNARE complex formation between Y- and V- or X- and U-SNAREs on the vesicle and their counterpart on the membrane of the target organelle as implemented in the original model (Heinrich and Rapoport, 2005) (reaction 8 in Table 1 and Figure 1A). SNARE-complex formation is catalyzed by tethering complexes that consist of cytoplasmic and/or peripheral membrane proteins (Dubuke and Munson, 2016; Hong and Lev, 2014). The fusion rate constant in the original model can be interpreted as a tethering rate constant. Our model extends the original model by the introduction of vesicle(v)- and target(t)-SNAREs (Jahn and Scheller, 2006) as well as a site and SNARE-specific tethering machinery (Dubuke and Munson, 2016; Hong and Lev, 2014). We define that SNAREs V- and U are v-SNAREs and SNAREs Y- and X t-SNAREs. By lowering the affinity of the t-SNAREs for the coat protein that mediates the budding of the vesicles that would bring the SNAREs back to the donor organelle, we ensure that mainly v-SNAREs are back transported, while t-SNAREs stay at the target organelle (Table 1). Consequently, budding vesicles mainly contain v-SNAREs that form complexes with their t-SNARE counterpart at the target membrane. Specificity of the tethering machinery at different locations is achieved by specifying different tethering rates for the two complementary sets of SNAREs, X and U SNARE complexes form with a higher tethering rate constant at the TGN, while Y and V SNARE complexes form with a higher tethering rate constant at the growth cone. The assumed reaction rates for the interactions between the coat proteins and other proteins involved in transport are given in Table 2

Based on their trafficking behavior, membrane proteins involved in neurite growth can be classified as stationary and cycling membrane proteins. Stationary proteins, i.e. recruitment factors and t-SNAREs, reside either at the TGN or GC, while cycling proteins, i.e. v-SNAREs and motor protein receptors, are continuously transported back and forth between the TGN and the GC. These different movement capabilities are presented in our model by different affinities of the membrane proteins for the coat proteins (Table 1). The affinity of stationary proteins towards the coat proteins involved in back transport is lower than the affinity of cycling proteins, ensuring that only cycling proteins are back transported to the donor organelle.

It should be noted that our model like the original model does not track individual vesicles, but assumes that all vesicles of one type (i.e. those vesicles that bud from the same donor membrane with the same coat protein) form a combined unit in the cytoplasmic compartments between the organelles. Biologically, this is based on the assumption that there is rapid and un-limited diffusion of all vesicle proteins between all vesicles of the same type. Once a vesicle buds from the TGN or GC, the concentration of all its membrane proteins immediately equilibrates with the concentration of the protein components of all other vesicles of the same set in the same cytoplasmic compartment. We think that this assumption is reasonable, since overall there should

bioRxiv preprint doi: https://doi.org/10.1101/153569; this version posted June 23, 2017. The copyright holder for this preprint (which was not certified by peer review) is the author/funder. All rights reserved. No reuse allowed without permission.

be no differences between the protein content of newly budded vesicles and previously budded vesicles.

Microtubule growth related SCPs

Microtubule (MT) dynamics are modeled as a one compartment model (Figure 1B, Table 3). Microtubules within neurites consist of dynamic and stable microtubules (Brady et al., 1984; Kollins et al., 2009; Song et al., 2013; Witte et al., 2008). Dynamic MTs are characterized by periods of MT growth and catastrophic breakdown (Suppl. Fig 2a), the latter can either lead to MT disappearance or be rescued, followed by a new growth period. The time frame of these periods is in seconds or minutes. Stable MTs do not show such periodic growth behavior and are assumed to have a constant length. Dynamic MTs are continuously generated at a specified nucleation rate (Reaction 9 in Table3, Suppl. Fig. 2F). The length of dynamic MTs (Reaction 10, Table 3) as well as the rate of MT catastrophic breakdowns depends on the effective tubulin concentration (Reaction 11 Table 3), i.e. the concentration of free tubulin that is available for polymerization and not sequestered by any other proteins (Curmi et al., 1997; Jourdain et al., 1997; Manna et al., 2009) (Suppl. Figure 2A-D). To characterize these relationships, we ran an initial set of simulations of the growth dynamics of a single dynamic MT using a published model (Margolin et al., 2012). Since we simulate NOG over hours and days, while dynamic MT growth behavior changes in seconds and minutes, we do not simulate individual dynamic MTs, but the whole population of dynamic MTs. To simulate the behavior of the whole dynamic MT population, we developed two formulas based on the results of the Margolin model. One formula describes the dependence of the average growth length of dynamic MTs on the effective tubulin concentration (Reaction 10 in Table 3, Suppl. Figure 2D), the other the dependence of the catastrophic breakdown rate that leads to complete disappearance of the dynamic MT on the effective tubulin concentration (Reaction 11 in Table 3, Suppl. Figure 2E). The count of dynamic MTs depends on the nucleation rate, the degradation rate due to catastrophic breakdown and the conversion rate into stable MTs (Reaction 12 in Table 3, Suppl. Figure 2F). We do not track the number of stable MTs, but the combined length of all stable MTs. The increase in length during conversion is calculated by the product of the average length of the dynamic MTs and the number of converted dynamic MTs (Reaction 13 in Table 3). The combined length of the dynamic MTs is the product of the number of dynamic MTs and the average length of the dynamic MTs (Reaction 14 in Table 3). To calculate the length of the microtubule scaffold within the neurite, the sum of the combined lengths of the dynamic and stable MTs is divided by the number of MTs per neurite cross-section (Reaction 15 in Table 3). An axon contains about 10 - 100 MTs per cross-section (Fadic et al., 1985). Since we simulate initial NOG we selected 20 MTs as the number of MTs per neurite cross-section in our model.

Growth of Neurite shaft

Vesicles that fuse with the GC deliver their membrane to the GC increasing the GC surface area. In our model we set the surface area of the GC of the growing neurite to 50 μm^2 (Kunda et al.,

bioRxiv preprint doi: https://doi.org/10.1101/153569; this version posted June 23, 2017. The copyright holder for this preprint (which was not certified by peer review) is the author/funder. All rights reserved. No reuse allowed without permission.

2001; Ren and Suter, 2016). Any membrane surface area that is added to the GC and would increase its size over 50 μm^2 is added to the neurite shaft. Membrane proteins are not added to the neurite shaft, since our model is based on the assumption that the diffusion of the membrane proteins into the neurite shaft is prevented by intra-membranous diffusion barriers or the interaction with cortical cytoskeleton proteins, such as PDZ-domain containing scaffold proteins (Ye and Zhang, 2013) that ensure a highly specialized growth cone membrane. The neurite shaft is modeled as a cylinder, allowing an easy calculation of the length of the neurite shaft based on its membrane surface area (Reaction 16 in Table 3). Since the MTC lies within the neurite shaft, its length is defined by the length of the neurite shaft, i.e. the length of the MTC continuously increases with the growing neurite

EXPERIMENT

Neurite outgrowth occurs at varying velocities

In primary cultures, neurons put out neurites at varying rates. To quantify the variability and determine the velocities with which the neurites grow we used a high content imaging system (IN Cell Analyzer) to track neurite outgrowth in primary rat cortical neurons. The experimentally observed velocities of neurite outgrowth could be used as top-down constraint for our model. We incubated rat cortical neurons for 16h and then documented neurite outgrowth every 6h. for additional 48h. The neurons with shortest and longest neurite were identified and their length quantified. Representative images at selected time points are shown in Figure 2A and 2B and a complete set of images is shown in Supplementary Figure 1. The neurons with shortest and longest neurite were identified and their length quantified. At each time point the neurites significantly differed in their lengths (Sup. Figure 1B). We used all the neurons in a field such as that shown in Sup Fig 1B and identified the length of selected quantiles and calculated the growth velocity for these quantiles. Median values are plotted in Figure 2C. The neurite growth velocities ranged from 0 to ~20 µm/h. We used these velocities as top-down whole cell response constraint in modeling the activities of the two different types of SCPs. Increases in the whole cell response, i.e. neurite outgrowth velocity depends on the coordinated increase of membrane production and delivery of membrane vesicles to the growth cone as well as microtubule growth. Both types of SCPs need to grow with the same velocity, since they are interdependent. Vesicles transport is microtubule dependent and microtubule growth is limited by the length of the neurite shaft. Similarly, the increase in membrane production needs to be coordinated with an increased vesicular transport. More vesicles would need to bud from the TGN, to be actively transported through the MTC and to fuse with the GC. These interdependencies form the basis for our top down constraint.

Postulates governing SCP dynamics

Within the overall constraint that the velocities of the two types of SCPs need to be balanced we used experimental data from the literature for additional constraints as the level of SCPs. These

bioRxiv preprint doi: https://doi.org/10.1101/153569; this version posted June 23, 2017. The copyright holder for this preprint (which was not certified by peer review) is the author/funder. All rights reserved. No reuse allowed without permission.

constraints arise from a set of postulates of permissible SCP functions that are described in Supplementary Table 1. We postulate that about ~10% of the anterograde vesicles in the MTC are bound to the MTC and actively moving along the microtubule (Ahmed and Saif, 2014). The other 90% constitute a membrane pool that could be recruited on demand to adapt to short term increases in outgrowth velocity. Similarly, we assume that the vesicles that reside in the growth cone (Erturk et al., 2007) are the first membrane reservoir for the quick recruitment of additional membrane and also define - in the same way - that 10% of the anterograde vesicles in the growth cone cytoplasm move, i.e. fuse with the growth cone membrane. This assumption is based on the experimental observation that GC membrane precursor vesicles reside in the GC cytoplasm before fusion with the membrane with a half-life of >/= 14min (Pfenninger et al., 2003), which would suggest that around 5% of the vesicles fuse with the membrane. Similarly, we assume that 90% of the retrograde vesicles in the MTC and the cell body cytoplasm are moving. The total growth cone membrane is completely internalized within 30 - 60 min (Diefenbach et al., 1999) which be based on a endocytosis rate between 0.833 μm^2/min and 1.66 μm^2/min for a growth cone with a surface area of 50 μm^2 (Kunda et al., 2001; Ren and Suter, 2016). Based on these observations and the assumption that some of the endocytosed vesicles might be part of transcytotic re-arrangements during growth cone steering (Tojima and Kamiguchi, 2015) or are transported to other growth cones and not to the cell body (Denburg et al., 2005), we set the rate of membrane back transport from the growth cone to the TGN to 0.5 μm^2/min. The back transported membrane can also be called cycling membrane, since it continuously cycles between the TGN and the growth cone without being added to the neurite shaft. For the microtubules we postulate that dynamic MTs should fill up 20 µm of the growing neurite. This is the length of the minor processes (Yu and Baas, 1994) that are characterized by continuous retraction and extension periods (Arimura and Kaibuchi, 2007). We assume that such periods are committed by continuous MT growth and retraction, so that the MT scaffold in these processes should mainly consist of dynamic MTs.

Using these constraints we ran simulations to identify an initial solution at one intermediate rate of neurite outgrowth or relationships between the coordinated activities of the different SCPS within each type of SCP and between SCPs. From these initial simulations we developed an overall analytical approach that allows us to predict the relationships that allow neurite outgrowth at a specified velocity.

SIMULATIONS AND ANALYTICAL ANALYSES

We identified a set of parameters that generated neurite outgrowth with a velocity of 5 µm/h (Figure 3, Suppl. Figure 3). Under steady state (Figure 3A), neurite surface area continuously increased with a rate of 0.2618 μm^2/min, (Figure 3B) in agreement with the amount of membrane that is needed to increase the length of the neurite (Figure3B) for the growing neurite. The vesicles in the MTC increased in parallel with a rate of ~0.22 vesicles/min assuming

bioRxiv preprint doi: https://doi.org/10.1101/153569; this version posted June 23, 2017. The copyright holder for this preprint (which was not certified by peer review) is the author/funder. All rights reserved. No reuse allowed without permission.

a membrane area of 0.05 μm^2 per vesicle (Figure 3C).The length of the microtubule bundles also increases proportionally to maintain the shaft growth rate (Figure 3D). For this we selected an effective tubulin concentration of 9 µM to achieve a length increase of the microtubule bundles with a velocity of 5µm/h. In considering the values of the ordinate for the different SCPs in Figure 3 it became clear that there are multiple combinations of kinetic parameters and amounts of components that allow neurite outgrowth at the same velocity without violating the constraints we imposed on dynamics of the SCPs.

To enable a systematic analysis of the redundancies within and between SCPs, we generated an analytical solution (Figure 4A) that predicts sets of parameter and protein amounts in the different compartments that enable neurite outgrowth at a fixed velocity of choice without violating constraints on SCP dynamics (Suppl. Table 1). In our solution, we consider that an increase in neurite outgrowth depends on varying sets of protein amounts and kinetic parameters that allow increased anterograde net transport of membrane vesicles and continuous synthesis of new proteins and membrane to compensate for the 'consumption' within the growing MTC. In addition to the postulated constraints on SCP dynamics we pre-define independent protein amounts and kinetic parameters (Fig 4A, right side) to calculate the dependent protein amounts and kinetic parameters.

The development of the analytical solution starts with the consideration of the final destination of the trafficking membrane (Figure 4B). Membrane that is incorporated into vesicles that bud from the TGN can be separated into 4 different membrane types. These membrane types should not be confused with the four different vesicle sets in our model that distinguish the vesicles based on the organelle they budded from and the coat protein they budded with (Figure 1A). Membrane of the first type will be added to the growing MTC as part of the MTC reservoir for anterograde moving vesicles. Membrane of the second type will be added to the GC and from there to the growing neurite shaft. Membrane of the third and fourth types will also be added to the GC, but the fused membrane will be incorporated into endocytic retrograde vesicles. Similarly to the first membrane set, the third set will be added to the growing MTC, though this set is much smaller due to an assumed nine-fold lower amount of stationary retrograde vesicles in the MTC. The fourth membrane set will be back transported to the TGN, i.e. this set constitutes the cycling membrane between the TGN and the GC. For simplification, we assume in our solution that membranes transported in an anterograde manner is only transported as vesicles that bud from the TGN with coat protein B and retrogradely transported membranes are vesicles that bud from the GC with coat protein A.

The specification of an NOG velocity, the amount of cycling membrane and the percentages of stationary anterograde and retrograde vesicles in the MTC allows the calculation of the fluxes of the 4 different membrane types. Based on these, the membrane production rate at the TGN as well as the budding rates at the TGN and GC can be calculated. The membrane production rate at the TGN is the sum of the fluxes of the first three membrane types, i.e. all membrane types that are not back transported to the TGN. The budding rate at the TGN (or initial forward transport

bioRxiv preprint doi: https://doi.org/10.1101/153569; this version posted June 23, 2017. The copyright holder for this preprint (which was not certified by peer review) is the author/funder. All rights reserved. No reuse allowed without permission.

rate) is the sum of all 4 fluxes and the endocytosis rate (or initial backward transport rate) is the sum of the fluxes of the third and fourth types. The fluxes also allowed us to calculate the initial membrane surface areas in the cytoplasmic compartments. Similarly to the fraction of anterograde vesicles that are bound to the microtubule and therefore moving in the MTC, we define the fractions of moving anterograde vesicles in the GC cytoplasm (i.e. vesicles that fuse with the GC membrane) and moving retrograde vesicles in the CB cytoplasm (i.e. vesicles that fuse with the TGN) (Table 4). The anticipated membrane fusion rate at the growth cone (or final forward transport rate) is equal to the sum of the fluxes of the second, third and fourth membrane types, the anticipated membrane fusion rate at the TGN (or final backward transport rate) is equal to the flux of the fourth membrane type. This allows the calculation of the amount of v-SNAREs that are associated with each set of vesicles in both cytoplasmic compartments. We are looking for that amount of v-SNAREs V in the GC cytoplasm or U in the CB cytoplasm that allows that the fractions of fusing vesicles equal the anticipated fractions and that the total membrane fluxes equal the final forward and final backward membrane fluxes under a pre-defined amount of t-SNAREs Y at the TGN and X at the GC and pre-defined tethering rates.

Vesicles that fuse with the TGN or the GC transmit their SNAREs to the target organelle. Consequently, the vesicles that enter the CB cytoplasm or GC cytoplasm from the MTC should contain the same amount of SNAREs to keep the number of SNARE molecules in the cytoplasmic compartments constant. Additionally, v-SNAREs need to be back transported to the GC or the TGN to be available for the next set of budding vesicles. The fluxes for each v-SNARE can be associated to 4 different types in a similar manner as the membrane fluxes. Initial and final forward and backward fluxes can be calculated accordingly. SNAREs are recruited into the budding vesicles in a competitive manner, i.e. all 4 SNAREs compete with each other for the SNARE binding spots of the budding vesicles. The amounts of t-SNAREs Y and X at the GC and the TGN are predefined. Considering this we calculated the amount of v-SNAREs V and U at the TGN and GC that allow the calculated initial forward and backward v-SNARE fluxes.

We calculated the amount of motor protein receptors that are associated with anterograde and retrograde vesicles in the MTC that is necessary to allow the anticipated fraction of microtubule bound (i.e. moving) vesicles. This enabled the calculation of the motor protein receptors in the other cytoplasmic compartments and the amount of motor protein receptors at the TGN and GC in a similar manner as we did it for the v-SNAREs.

Finally, we calculated the fluxes for the stationary proteins, i.e. t-SNAREs X and Y and the recruitment factors 1 and 2 as well as the initial protein amounts in the different cytoplasmic compartments.

For the calculation of initial amounts of all membrane proteins in the different cytoplasmic compartments, we first calculated the concentration of all membrane proteins in anterograde and retrograde moving vesicles. The initial amounts were obtained by multiplication of the initial membrane amounts in the different compartments and the protein concentrations.

bioRxiv preprint doi: https://doi.org/10.1101/153569; this version posted June 23, 2017. The copyright holder for this preprint (which was not certified by peer review) is the author/funder. All rights reserved. No reuse allowed without permission.

The 'consumption' of membrane proteins that are associated with the vesicles that are added to the MTC reservoir demands the continuous production of membrane proteins at the TGN. The protein production rates can be calculated by considering the concentration of each protein at anterograde and retrograde moving vesicles and the amount of membrane that will be added to the MTC reservoir.

For the calculation of the rates that determine MT growth with a fixed velocity of choice we specified the effective tubulin concentration (that determines the length of the dynamic MTs and the degradation rate of dynamic MTs) and the length of the dynamic MTs. Based on these values the nucleation rate for dynamic MTs and the conversion rate of dynamic into stable MTs were calculated.

The analytical solution was validated by comparing the analytically predicted outcome with the results of the numerical simulation for example sets of parameter and protein amounts (Figs. 4C and D, suppl. figure 4). We used the predicted parameter and protein amount sets as starting points in our model and run the numerical simulation for 5000 minutes (~3.5 days). Every 1000 min we compared the anticipated model constraints with the numerically obtained values to estimate the accuracy of our analytical prediction. The analytical solution matched the anticipated model constraints with high accuracy, except the fusion rate for retrograde vesicles with the TGN that for was too high for the velocities 0 and 2.5 µm/h.

We also investigated the impact of un-coordinated SCP activities on steady NOG at a fixed velocity by mixing up the predicted parameters and initial protein amounts that were obtained for two analytical solutions based on two different NOG velocities. We used the initial protein amounts, parameters and membrane production rates that were obtained based on a NOG velocity of 10 µm/h, while protein production rates were predicted based on a NOG velocity of 5 µm/h. This example simulates the mismatch between protein production for different SCPs and membrane generation and delivery to the growth cone. Although initially the neurite growth occurred with the anticipated velocity of 10 µm/h, the lack of replacement of proteins that are used in the growing MTC significantly decreased the outgrowth velocity to 5 µm/h, while overloading the MTC, the cell body and growth cone cytoplasm with stationary vesicles, as shown by the decreasing level of moving vesicles in the different compartments (Figure 5).

Interplay between cycling and stationary components for membrane delivery

We used the analytical solution to investigate the relationship between the different components of our dynamical model. As described, some components, such as v-SNAREs and motor protein receptors fulfill their function within the vesicle movement SCP. These proteins cycle between the TGN and the GC membrane, because they need to be brought back to the donor organelle to be available for new budding vesicles. Other components, such as the cytoplasmic tethering machinery or t-SNAREs reside at their local destination. We were particularly interested in the

bioRxiv preprint doi: https://doi.org/10.1101/153569; this version posted June 23, 2017. The copyright holder for this preprint (which was not certified by peer review) is the author/funder. All rights reserved. No reuse allowed without permission.

relation between the stationary and cycling components that are associated with anterograde moving vesicle, i.e. v-SNAREs V and tethering in the growth cone and kinesin receptor and kinesin dissociation constant at the microtubule.

We generated multiple tethering rates and identified the total amount of vesicle(v)-SNARE V that results in the forward fusion of a sufficient amount of vesicles allowing neurite outgrowth with the anticipated velocity without violation of the target outputs (under the assumption of a tethering rate for SNAREs X and U at the TGN of $8x10^{-6}$ /molecule). We did not change the t-SNARE Y amount, since its influence on SNARE-complex formation should be similar to the influence of the tethering machinery. Our algorithm identified a hyperbolic relationship between the tethering rate and the amount of v-SNAREs that increases to higher values with faster velocities (Figure 6A). Our results indicate that at high tethering rates (e.g. $4x10^{-6}$/molecule), the switch between different velocities is facilitated by only small changes in the v-SNAREs, while at high v-SNARE amounts (e.g. $2x10^{4}$ molecules) the switch between different velocities is facilitated by only small changes in the tethering rates. The synthesis rate of the v-SNARE V that is necessary to compensate for the consumption of SNARE V by the growing MTC increases with decreasing tethering rates (Figure 6B) because of the higher base line level for the SNARE V at the start of neurite outgrowth. On the other hand, our simulations reveal that an increase in growth velocity is associated with an over proportional increase in the synthesis rate of SNARE V. The higher the rate of membrane delivery to the growth cone tip, the more vesicles need to be transported along the MTC, increasing the density of vesicles at the MTC. Since only 10% of all vesicles are moving along the microtubule, an increased density is directly transferred to an increase in vesicles in the MTC reservoir, explaining the over proportional increase of the production rates for SNARE V. Such an over proportional increase in production rates might come along with high energy consumption by the gene expression machinery, so that at higher velocities the neuron might reduce the size of the membrane reservoir in its MTC to keep outgrowth costs within reasonable ranges.

An analysis of the other protein amounts at start of neurite outgrowth showed small variations or no changes in the protein amounts as a function of the tethering rate at the growth cone membrane (Suppl. Figure 5). An increase in outgrowth velocity was associated with an increase in initial protein amounts of the motor protein receptors, did not change the initial amounts of the stationary t-SNAREs and recruitment factors and decreased the initial amount of the v-SNARE U that mediates vesicle fusion at the TGN. The decrease of the initial amount of the v-SNARE U can be explained by the increased number of anterograde moving vesicles, that provide more binding spots for SNARE U. Since under a constant cycling rate the number of retrograde moving vesicles stays constant with increasing outgrowth velocity, the amount of SNARE U that needs to brought back to the growth cone to be available for endocytosed vesicles is independent of the outgrowth velocity. However, increasing anterograde moving vesicles decrease the amount of SNARE U per anterograde vesicle, lowering the SNARE U concentration at the TGN that is needed to load anterograde vesicles with the needed amount of SNARE U.

bioRxiv preprint doi: https://doi.org/10.1101/153569; this version posted June 23, 2017. The copyright holder for this preprint (which was not certified by peer review) is the author/funder. All rights reserved. No reuse allowed without permission.

In contrast to the synthesis rate of the v-SNARE V all other production rates are independent of the tethering rate in the growth cone (suppl. Figure 5). The production rate for all cycling proteins increase with an increase in outgrowth velocity, while there almost no for additional synthesis of stationary proteins. Interestingly, the increase in proteins that function in retrograde vesicle transport (e.g. dynein receptors and v-SNARE U) linearly increase with increasing outgrowth velocity in contrast to the nonlinear increase of the proteins that function in anterograde vesicle transport.

Next, we investigated the relationship between the stationary kinesin dissociation constant and the amount of the cycling molecule kinesin (Figure 6C). We identified a similar hyperbolic relationship that was identified for the tethering rate and the v-SNARE V, giving rise to the same conclusions about the robustness of the system towards fluctuations. The needed synthesis rate for kinesin increased over proportionally with the outgrowth velocity and depended on the kinesin dissociation constant, as it was documented for the v-SNARE V and the tethering rate (Figure 6D). One might consider that in contrast to the tethering rate, the fraction of MT-bound kinesin refers to components along the whole MTC, while the tethering rate describes components that are locally restricted to the growth cone.

Microtubule growth is regulated via effective tubulin and the nucleation rate

Microtubule growth velocity is determined by the nucleation rate for new dynamic MTs, the length of the dynamic MTs and the degradation of dynamic microtubules that both depend on the effective tubulin concentration and the conversion rate of dynamic MTs into stable MTs. At steady state, the nucleation of new dynamic microtubules is equal to the degradation of dynamic MTs and the conversion of dynamic into stable MTs. The more MTs nucleate, the more MTs will be converted into stable MTs, increasing the growth velocity of the microtubule scaffold. Similarly, the higher the effective tubulin, the lower the degradation rate and the longer the dynamic MTs as well as the converted dynamic MTs (Fig. 7A), also increasing the growth velocity of the microtubule scaffold. We documented the relation between the effective tubulin concentration and the nucleation rate that allow neurite outgrowth with a certain velocity and identified a hyperbolic relationship between both entities (Fig 7B). The lower the nucleation rate, the more effective tubulin is needed to maintain a certain outgrowth velocity, but the less additional effective tubulin is needed to increase the outgrowth velocity. Multiple mechanisms regulate the sequestration of tubulin (Arimura and Kaibuchi, 2007) and thereby its availability for polymerization. Sequestered tubulin might function as a similar reservoir for increased outgrowth on demand as we proposed for the vesicles in the MTC. By releasing sequestered tubulin on demand, the neuron might be able to increase its outgrowth velocity without the need for additional synthesis of tubulin or the components of tubulin nucleation centers. The available nucleation rate determines the sensitivity of microtubule scaffold growth towards changes in the effective tubulin concentration and has an impact on the distinction between noisy fluctuations in the effective tubulin concentration and wanted regulations. Since the average length of the dynamic microtubules increases exponentially with the effective tubulin concentration (Fig 6A),

bioRxiv preprint doi: https://doi.org/10.1101/153569; this version posted June 23, 2017. The copyright holder for this preprint (which was not certified by peer review) is the author/funder. All rights reserved. No reuse allowed without permission.

our model suggests that the sensitivity of the microtubule scaffold towards effective tubulin also increases with the effective tubulin concentration itself.

Discussion

Neurite outgrowth depends on the coordinated activities of various sub-cellular processes. Of the different SCPs involved, the types of SCPs are critical. They are the SCPs that regulate vesicle traffic and microtubule dynamics. We developed a dynamical model that incorporates both types of SCPs and have documented that the activity of the SCPs involved need to be highly coordinated to allow neurite outgrowth at a certain velocity. To make the model more manageable our simulations were done under the assumption that (1) the size of the TGN (50 μm^2) is independent of the outgrowth velocity (2) that the rate of back transported membrane from the growth cone to the TGN is 0.5 μm^2/min, (3) that 90 % of the anterograde vesicles in the MTC and the growth cone cytoplasm serve as membrane reservoir (i.e. these vesicles are not moving) and (4) that 20 µm of the neurite microtubule scaffold consists of dynamic MTs and the rest of stable MTs. All of these assumptions are based on experimental data and allow us to identify the key features of the balance between SCP types required for a dynamic whole cell response. We could show that the activity of certain SCPs depends on each other, i.e. to achieve the same reservoir size and outgrowth velocity, an increase in the activity of one SCP is associated with a decrease in the activity of the other SCP. This accounts for the activity of the tethering machinery and the components of the SNARE complexes as well as for the kinesin binding to the microtubules and the amount of kinesin loaded on vesicle bound kinesin receptors. Our simulations propose that in both cases the cell can select between cell states that allow an increase in growth velocity by only small changes of one of the complementary SCPs or cell states that demand a similar increase in both of the complementary SCPs. The actual cell state might depend on multiple factors, among which are the amount of energy that needs to be invested into neurite outgrowth at a certain velocity, as well as the robustness of the system towards random fluctuations.

Since the size of the MTC grows with the growing neurite, the size of the reservoir within it also grows. Therefore the maintenance of steady state conditions demands the continuous production of additional proteins and membrane (as membrane vesicles). We find that that the need for additional protein synthesis increases over-proportionally with increasing outgrowth velocity for those proteins that regulate anterograde vesicular transport (in particular v-SNARE V and the kinesin receptor). Such an increase might be associated with significant costs in form of energy consumption by the transcriptional and translational machinery. Our simulations suggest that the cell might reduce the size of the membrane reservoir with increasing outgrowth velocity and so it has a built in ability to further increase the outgrowth velocity for a short time period upon demand.

bioRxiv preprint doi: https://doi.org/10.1101/153569; this version posted June 23, 2017. The copyright holder for this preprint (which was not certified by peer review) is the author/funder. All rights reserved. No reuse allowed without permission.

Microtubule growth depends on the nucleation rate and the effective tubulin concentration, i.e. free tubulin that is available for polymerization and not sequestered by cytoplasmic proteins. Such sequestration could serve as a tubulin reservoir, similar to the proposed membrane vesicle reservoir function of the MTC and GC cytoplasm. The nucleation rate determines the sensitivity of the microtubule growth towards effective tubulin concentration changes. Our simulations suggest that the sensitivity also increases with increasing effective tubulin concentrations, since the length of the dynamic MTs increase exponentially with the effective tubulin concentration.

Multiple mechanisms regulate tubulin sequestration by stathmin, including signaling mechanisms that involve PTEN and GSK3β (Arimura and Kaibuchi, 2007). Interestingly, the same signaling mechanisms could also control the activity of the tethering machinery (Lalli, 2009; Sugihara et al., 2002), suggesting the coordinated regulation of both – membrane vesicle availability and tubulin mobilization - by the same input signals. The appearance of a neurite guidance factor might activate these mechanisms, leading to the coordinated mobilization of tubulin and membrane vesicle from both reservoirs, to trigger an immediate push of the neurite into the anticipated direction.

Overall, this model provides deep new insight into how classes of subcellular processes need to be coordinately regulated to enable a whole cell function in a manner that is experimentally observed. Although we do not know many of the individual kinetic parameters or protein levels, parameter variation exercises indicate that key features of systems level regulation can be understood without precise knowledge of individual reaction rates or protein levels, although knowing all the values will be valuable in bringing greater realism to this model and increasing of understanding how molecule to cell level scaling mechanisms work. In spite of these limitations this study shows that putting to together various in-depth studies of SCPs can allow us to observe deep insight how the balance between lower level dynamic processes required for cell level dynamic functions.

Acknowledgements: This research was supported by NIH grant GM54508 and the Systems Biology Center grant GM 071558. We thank Alan Stern and Marc Birtwistle with help in image acquisition using the InCell analyzer.

Author contributions: R.I. and J.H. conceived the project. A.Y. and J.H. developed and implemented the model. V.R. and M.S. prepared rat cortical neurons. A.Y. analyzed the images. A.Y., R.I. and J.H. wrote the manuscript.

bioRxiv preprint doi: https://doi.org/10.1101/153569; this version posted June 23, 2017. The copyright holder for this preprint (which was not certified by peer review) is the author/funder. All rights reserved. No reuse allowed without permission.

References

Ahmed, W.W., and Saif, T.A. (2014). Active transport of vesicles in neurons is modulated by mechanical tension. Scientific reports *4*, 4481.

Arimura, N., and Kaibuchi, K. (2007). Neuronal polarity: from extracellular signals to intracellular mechanisms. Nature reviews Neuroscience *8*, 194-205.

Azeloglu, E.U., Hardy, S.V., Eungdamrong, N.J., Chen, Y., Jayaraman, G., Chuang, P.Y., Fang, W., Xiong, H., Neves, S.R., Jain, M.R*., et al.* (2014). Interconnected network motifs control podocyte morphology and kidney function. Science signaling *7*, ra12.

Bhalla, U.S., and Iyengar, R. (1999). Emergent properties of networks of biological signaling pathways. Science *283*, 381-387.

Black, M.M., Slaughter, T., Moshiach, S., Obrocka, M., and Fischer, I. (1996). Tau is enriched on dynamic microtubules in the distal region of growing axons. The Journal of neuroscience : the official journal of the Society for Neuroscience *16*, 3601-3619.

Brady, S.T., Tytell, M., and Lasek, R.J. (1984). Axonal tubulin and axonal microtubules: biochemical evidence for cold stability. J Cell Biol *99*, 1716-1724.

Brodsky, F.M. (2012). Diversity of clathrin function: new tricks for an old protein. Annual review of cell and developmental biology *28*, 309-336.

Burgo, A., Proux-Gillardeaux, V., Sotirakis, E., Bun, P., Casano, A., Verraes, A., Liem, R.K., Formstecher, E., Coppey-Moisan, M., and Galli, T. (2012). A molecular network for the transport of the TI-VAMP/VAMP7 vesicles from cell center to periphery. Developmental cell *23*, 166-180.

Collins, A., Warrington, A., Taylor, K.A., and Svitkina, T. (2011). Structural organization of the actin cytoskeleton at sites of clathrin-mediated endocytosis. Current biology : CB *21*, 1167-1175.

Curmi, P.A., Andersen, S.S., Lachkar, S., Gavet, O., Karsenti, E., Knossow, M., and Sobel, A. (1997). The stathmin/tubulin interaction in vitro. The Journal of biological chemistry *272*, 25029-25036.

Denburg, J.L., Hughen, R.W., Tucker, D., and Kater, S.B. (2005). Fate of constitutive endocytic vesicles formed in the growth cone: transport of vesicles from one growth cone to another in the same neuron. Journal of neurobiology *62*, 262-277.

Diefenbach, T.J., Guthrie, P.B., Stier, H., Billups, B., and Kater, S.B. (1999). Membrane recycling in the neuronal growth cone revealed by FM1-43 labeling. The Journal of neuroscience : the official journal of the Society for Neuroscience *19*, 9436-9444.

Dixit, R., Ross, J.L., Goldman, Y.E., and Holzbaur, E.L. (2008). Differential regulation of dynein and kinesin motor proteins by tau. Science *319*, 1086-1089.

Dubuke, M.L., and Munson, M. (2016). The Secret Life of Tethers: The Role of Tethering Factors in SNARE Complex Regulation. Frontiers in cell and developmental biology *4*, 42.

Ebneth, A., Godemann, R., Stamer, K., Illenberger, S., Trinczek, B., and Mandelkow, E. (1998). Overexpression of tau protein inhibits kinesin-dependent trafficking of vesicles, mitochondria, and endoplasmic reticulum: implications for Alzheimer's disease. The Journal of cell biology *143*, 777-794.

Ehrlich, M., Boll, W., Van Oijen, A., Hariharan, R., Chandran, K., Nibert, M.L., and Kirchhausen, T. (2004). Endocytosis by random initiation and stabilization of clathrin-coated pits. Cell *118*, 591-605.

Encalada, S.E., Szpankowski, L., Xia, C.H., and Goldstein, L.S. (2011). Stable kinesin and dynein assemblies drive the axonal transport of mammalian prion protein vesicles. Cell *144*, 551-565.

Erturk, A., Hellal, F., Enes, J., and Bradke, F. (2007). Disorganized microtubules underlie the formation of retraction bulbs and the failure of axonal regeneration. The Journal of neuroscience : the official journal of the Society for Neuroscience *27*, 9169-9180.

Fadic, R., Vergara, J., and Alvarez, J. (1985). Microtubules and caliber of central and peripheral processes of sensory axons. The Journal of comparative neurology *236*, 258-264.

bioRxiv preprint doi: https://doi.org/10.1101/153569; this version posted June 23, 2017. The copyright holder for this preprint (which was not certified by peer review) is the author/funder. All rights reserved. No reuse allowed without permission.

Fivaz, M., Bandara, S., Inoue, T., and Meyer, T. (2008). Robust neuronal symmetry breaking by Ras-triggered local positive feedback. Current biology : CB *18*, 44-50.

Fu, M.M., Nirschl, J.J., and Holzbaur, E.L. (2014). LC3 binding to the scaffolding protein JIP1 regulates processive dynein-driven transport of autophagosomes. Developmental cell *29*, 577-590.

Godlee, C., and Kaksonen, M. (2013). Review series: From uncertain beginnings: initiation mechanisms of clathrin-mediated endocytosis. The Journal of cell biology *203*, 717-725.

Gracias, N.G., Shirkey-Son, N.J., and Hengst, U. (2014). Local translation of TC10 is required for membrane expansion during axon outgrowth. Nature communications *5*, 3506.

Hagiwara, H., Yorifuji, H., Sato-Yoshitake, R., and Hirokawa, N. (1994). Competition between motor molecules (kinesin and cytoplasmic dynein) and fibrous microtubule-associated proteins in binding to microtubules. The Journal of biological chemistry *269*, 3581-3589.

Heinrich, R., and Rapoport, T.A. (2005). Generation of nonidentical compartments in vesicular transport systems. The Journal of cell biology *168*, 271-280.

Hong, W., and Lev, S. (2014). Tethering the assembly of SNARE complexes. Trends in cell biology *24*, 35-43.

Jahn, R., and Scheller, R.H. (2006). SNAREs--engines for membrane fusion. Nature reviews Molecular cell biology *7*, 631-643.

Jourdain, L., Curmi, P., Sobel, A., Pantaloni, D., and Carlier, M.F. (1997). Stathmin: a tubulin-sequestering protein which forms a ternary T2S complex with two tubulin molecules. Biochemistry *36*, 10817-10821.

Kempf, M., Clement, A., Faissner, A., Lee, G., and Brandt, R. (1996). Tau binds to the distal axon early in development of polarity in a microtubule- and microfilament-dependent manner. The Journal of neuroscience : the official journal of the Society for Neuroscience *16*, 5583-5592.

Kiddie, G., McLean, D., Van Ooyen, A., and Graham, B. (2005). Biologically plausible models of neurite outgrowth. Progress in brain research *147*, 67-80.

Kienzle, C., and von Blume, J. (2014). Secretory cargo sorting at the trans-Golgi network. Trends in cell biology *24*, 584-593.

Kim, K. (2016). Cargo trafficking from the trans-Golgi network towards the endosome. Biology of the cell *108*, 205-218.

Kollins, K.M., Bell, R.L., Butts, M., and Withers, G.S. (2009). Dendrites differ from axons in patterns of microtubule stability and polymerization during development. Neural Dev *4*, 26.

Kunda, P., Paglini, G., Quiroga, S., Kosik, K., and Caceres, A. (2001). Evidence for the involvement of Tiam1 in axon formation. The Journal of neuroscience : the official journal of the Society for Neuroscience *21*, 2361-2372.

Lajoie, P., and Nabi, I.R. (2007). Regulation of raft-dependent endocytosis. Journal of cellular and molecular medicine *11*, 644-653.

Lalli, G. (2009). RalA and the exocyst complex influence neuronal polarity through PAR-3 and aPKC. Journal of cell science *122*, 1499-1506.

LaPointe, N.E., Morfini, G., Pigino, G., Gaisina, I.N., Kozikowski, A.P., Binder, L.I., and Brady, S.T. (2009). The amino terminus of tau inhibits kinesin-dependent axonal transport: implications for filament toxicity. Journal of neuroscience research *87*, 440-451.

Lord, C., Bhandari, D., Menon, S., Ghassemian, M., Nycz, D., Hay, J., Ghosh, P., and Ferro-Novick, S. (2011). Sequential interactions with Sec23 control the direction of vesicle traffic. Nature *473*, 181-186.

Maday, S., Wallace, K.E., and Holzbaur, E.L. (2012). Autophagosomes initiate distally and mature during transport toward the cell soma in primary neurons. The Journal of cell biology *196*, 407-417.

Mandell, J.W., and Banker, G.A. (1996). A spatial gradient of tau protein phosphorylation in nascent axons. The Journal of neuroscience : the official journal of the Society for Neuroscience *16*, 5727-5740.

bioRxiv preprint doi: https://doi.org/10.1101/153569; this version posted June 23, 2017. The copyright holder for this preprint (which was not certified by peer review) is the author/funder. All rights reserved. No reuse allowed without permission.

Manna, T., Thrower, D.A., Honnappa, S., Steinmetz, M.O., and Wilson, L. (2009). Regulation of microtubule dynamic instability in vitro by differentially phosphorylated stathmin. The Journal of biological chemistry *284*, 15640-15649.

Margolin, G., Gregoretti, I.V., Cickovski, T.M., Li, C., Shi, W., Alber, M.S., and Goodson, H.V. (2012). The mechanisms of microtubule catastrophe and rescue: implications from analysis of a dimer-scale computational model. Molecular biology of the cell *23*, 642-656.

McNiven, M.A., and Thompson, H.M. (2006). Vesicle formation at the plasma membrane and trans-Golgi network: the same but different. Science *313*, 1591-1594.

Mettlen, M., and Danuser, G. (2014). Imaging and modeling the dynamics of clathrin-mediated endocytosis. Cold Spring Harbor perspectives in biology *6*, a017038.

Nakazawa, H., Sada, T., Toriyama, M., Tago, K., Sugiura, T., Fukuda, M., and Inagaki, N. (2012). Rab33a mediates anterograde vesicular transport for membrane exocytosis and axon outgrowth. The Journal of neuroscience : the official journal of the Society for Neuroscience *32*, 12712-12725.

Pfenninger, K.H. (2009). Plasma membrane expansion: a neuron's Herculean task. Nature reviews Neuroscience *10*, 251-261.

Pfenninger, K.H., Laurino, L., Peretti, D., Wang, X., Rosso, S., Morfini, G., Caceres, A., and Quiroga, S. (2003). Regulation of membrane expansion at the nerve growth cone. Journal of cell science *116*, 1209-1217.

Prager-Khoutorsky, M., and Spira, M.E. (2009). Neurite retraction and regrowth regulated by membrane retrieval, membrane supply, and actin dynamics. Brain research *1251*, 65-79.

Prevo, B., Mangeol, P., Oswald, F., Scholey, J.M., and Peterman, E.J. (2015). Functional differentiation of cooperating kinesin-2 motors orchestrates cargo import and transport in C. elegans cilia. Nature cell biology *17*, 1536-1545.

Ren, Y., and Suter, D.M. (2016). Increase in Growth Cone Size Correlates with Decrease in Neurite Growth Rate. Neural plasticity *2016*, 3497901.

Seitz, A., Kojima, H., Oiwa, K., Mandelkow, E.M., Song, Y.H., and Mandelkow, E. (2002). Single-molecule investigation of the interference between kinesin, tau and MAP2c. The EMBO journal *21*, 4896-4905.

Sochacki, K.A., Dickey, A.M., Strub, M.P., and Taraska, J.W. (2017). Endocytic proteins are partitioned at the edge of the clathrin lattice in mammalian cells. Nature cell biology *19*, 352-361.

Song, Y., Kirkpatrick, L.L., Schilling, A.B., Helseth, D.L., Chabot, N., Keillor, J.W., Johnson, G.V., and Brady, S.T. (2013). Transglutaminase and polyamination of tubulin: posttranslational modification for stabilizing axonal microtubules. Neuron *78*, 109-123.

Sugihara, K., Asano, S., Tanaka, K., Iwamatsu, A., Okawa, K., and Ohta, Y. (2002). The exocyst complex binds the small GTPase RalA to mediate filopodia formation. Nature cell biology *4*, 73-78.

Tojima, T., and Kamiguchi, H. (2015). Exocytic and endocytic membrane trafficking in axon development. Development, growth & differentiation *57*, 291-304.

Tsaneva-Atanasova, K., Burgo, A., Galli, T., and Holcman, D. (2009). Quantifying neurite growth mediated by interactions among secretory vesicles, microtubules, and actin networks. Biophysical journal *96*, 840-857.

Twelvetrees, A.E., Pernigo, S., Sanger, A., Guedes-Dias, P., Schiavo, G., Steiner, R.A., Dodding, M.P., and Holzbaur, E.L. (2016). The Dynamic Localization of Cytoplasmic Dynein in Neurons Is Driven by Kinesin-1. Neuron *90*, 1000-1015.

Vershinin, M., Carter, B.C., Razafsky, D.S., King, S.J., and Gross, S.P. (2007). Multiple-motor based transport and its regulation by Tau. Proceedings of the National Academy of Sciences of the United States of America *104*, 87-92.

Wang, T., Liu, Y., Xu, X.H., Deng, C.Y., Wu, K.Y., Zhu, J., Fu, X.Q., He, M., and Luo, Z.G. (2011). Lgl1 activation of rab10 promotes axonal membrane trafficking underlying neuronal polarization. Developmental cell *21*, 431-444.

bioRxiv preprint doi: https://doi.org/10.1101/153569; this version posted June 23, 2017. The copyright holder for this preprint (which was not certified by peer review) is the author/funder. All rights reserved. No reuse allowed without permission.

Wissner-Gross, Z.D., Scott, M.A., Ku, D., Ramaswamy, P., and Fatih Yanik, M. (2011). Large-scale analysis of neurite growth dynamics on micropatterned substrates. Integrative biology : quantitative biosciences from nano to macro *3*, 65-74.

Witte, H., Neukirchen, D., and Bradke, F. (2008). Microtubule stabilization specifies initial neuronal polarization. J Cell Biol *180*, 619-632.

Ye, F., and Zhang, M. (2013). Structures and target recognition modes of PDZ domains: recurring themes and emerging pictures. The Biochemical journal *455*, 1-14.

Yu, W., and Baas, P.W. (1994). Changes in microtubule number and length during axon differentiation. The Journal of neuroscience : the official journal of the Society for Neuroscience *14*, 2818-2829.

bioRxiv preprint doi: https://doi.org/10.1101/153569; this version posted June 23, 2017. The copyright holder for this preprint (which was not certified by peer review) is the author/funder. All rights reserved. No reuse allowed without permission.

Main Paper Figures and Tables:

Figure 1A

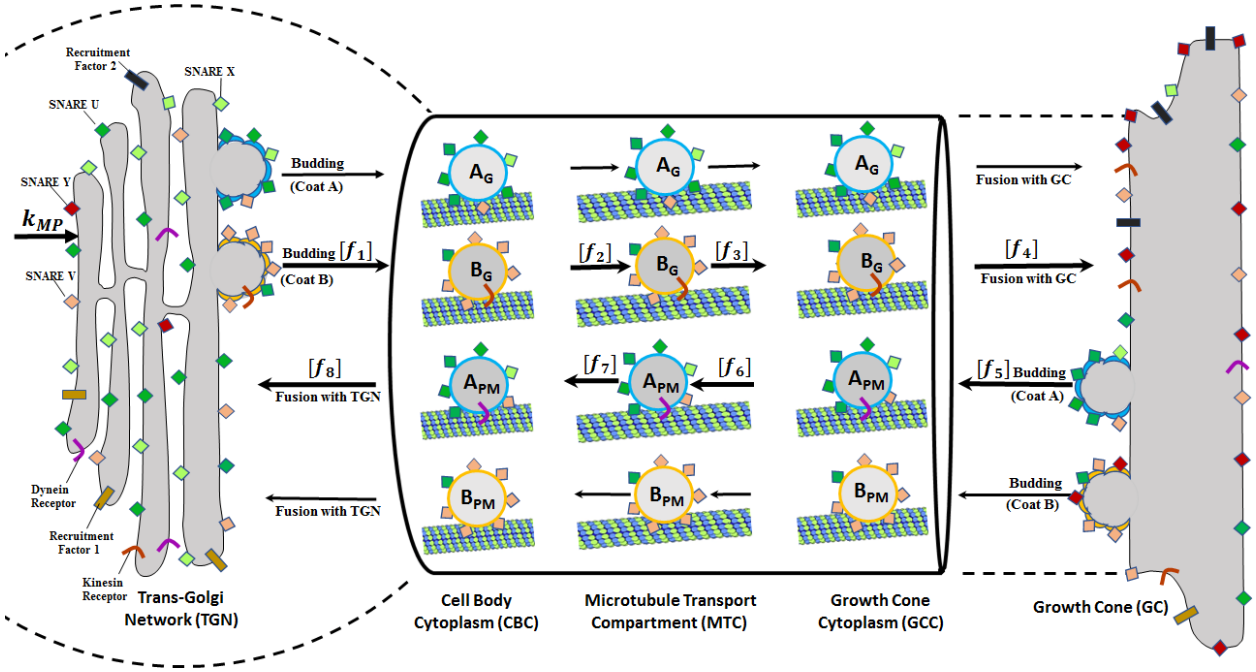

Figure 1B

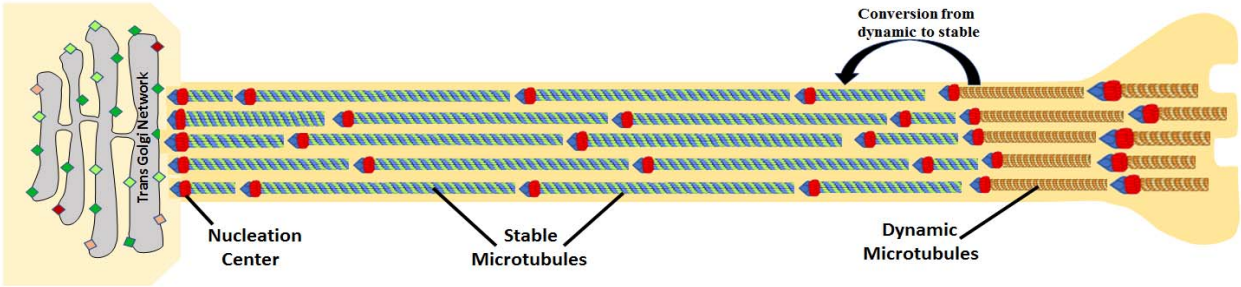

bioRxiv preprint doi: https://doi.org/10.1101/153569; this version posted June 23, 2017. The copyright holder for this preprint (which was not certified by peer review) is the author/funder. All rights reserved. No reuse allowed without permission.

Figure 1: Schematic description of dynamical model of vesicular transport and microtubule growth involved in neurite outgrowth. (A) Membrane delivery to the growth cone is modeled by use of an extended version of a dynamical model that describes vesicular transport between two different organelles (Heinrich and Rapoport 2006). In this model, new synthesized membrane is added to the Trans Golgi network (TGN) from where it is transported to the growth cone by vesicular transport. Vesicles bud from the TGN and are loaded on the microtubule for active kinesin mediated anterograde transport towards the growth cone where the membrane vesicles are delivered to growing neurite. The vesicles pass through three intermediate compartments: the cell body cytoplasm, the MTC and the growth cone cytoplasm. In each compartment kinesin has a different affinity for microtubules and is therefore associated with varying fractions of MT bound moving vesicles. Vesicles that are endocytosed from the growth cone move along the microtubule in the retrograde direction through dynein mediated active transport. Vesicle budding at the TGN or growth cone is mediated by the interaction of recruitment factors and coat proteins at the donor compartment, vesicle fusion by the formation of SNARE complexes between vesicle(v)-SNAREs and target(t)-SNAREs that is catalyzed by the tethering machinery. Motor proteins are bound to vesicles through motor protein receptors.**(B)** The dynamic model of microtubule growth consists of two different pools of microtubules, stable and dynamic microtubules. Dynamic microtubules alternate between growth, catastrophic breakdown and rescue that initiates another growth period. Nucleation leads to dynamic microtubules that are converted into stable microtubules. The length of the microtubule in the neurite shaft is the combined length of all dynamic and stable microtubules.

bioRxiv preprint doi: https://doi.org/10.1101/153569; this version posted June 23, 2017. The copyright holder for this preprint (which was not certified by peer review) is the author/funder. All rights reserved. No reuse allowed without permission.

Figure 2A

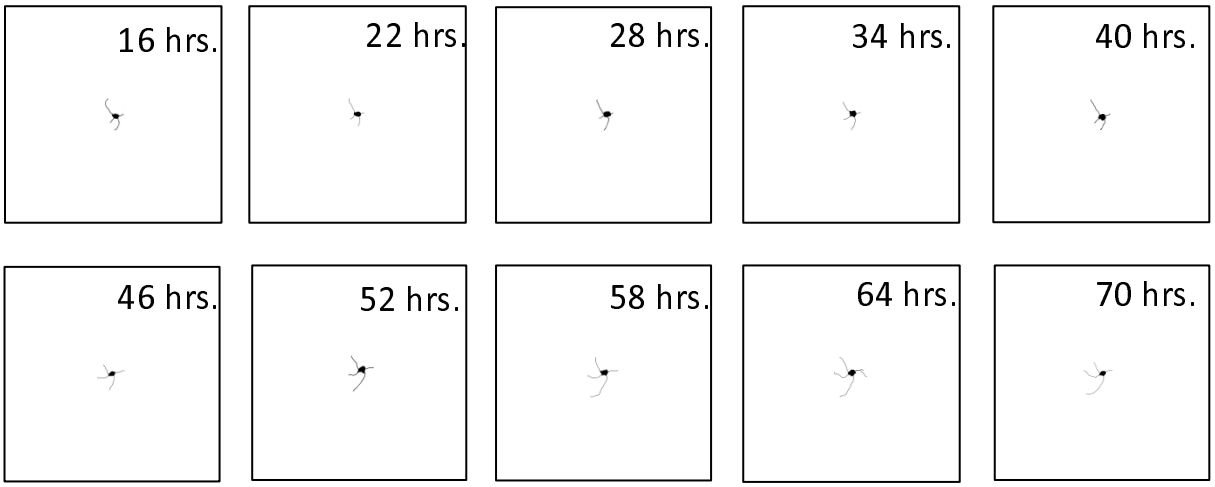

Slowly growing neurite

Figure 2B

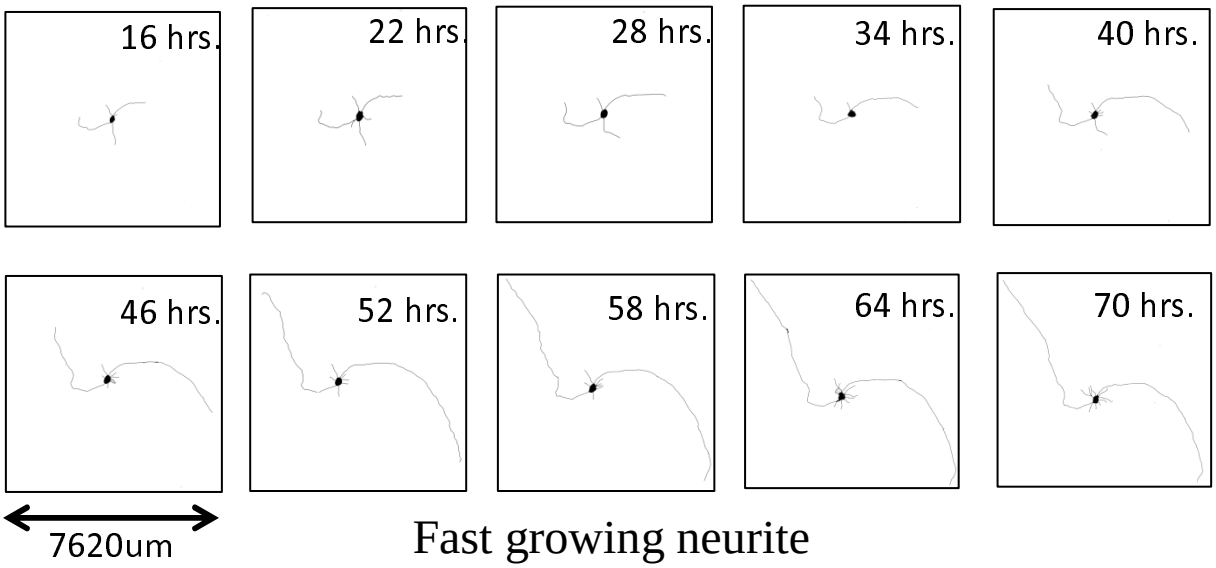

Fast growing neurite

bioRxiv preprint doi: https://doi.org/10.1101/153569; this version posted June 23, 2017. The copyright holder for this preprint (which was not certified by peer review) is the author/funder. All rights reserved. No reuse allowed without permission.

Figure 2C

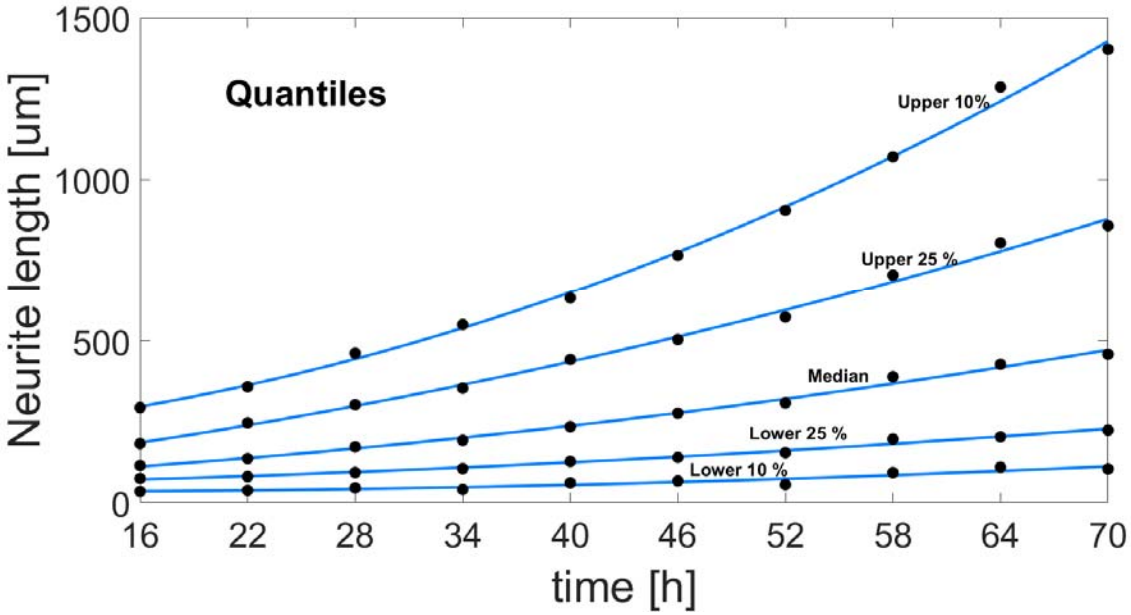

Figure 2: Neurites grow with different outgrowth velocities. Neurons were dissected from rat cortical brain, incubated for 16h to allow initial growth, followed by image acquisition every 6h up to 70h after plating. (A) Outgrowth of two selected neurons with short neurites over a 54h period. (B)Outgrowth of two selected neurons with long neurites over a 54h period. (C) For each neuron the length of the longest neurite was quantified at the indicated time points and the distribution of all lengths was evaluated. We selected the length of that neurite that matches the indicated quantiles at each timepoint. Linear interpolation of the lengths for each quantile documented outgrowth velocities varying from 0 to ~20 µm/h.

bioRxiv preprint doi: https://doi.org/10.1101/153569; this version posted June 23, 2017. The copyright holder for this preprint (which was not certified by peer review) is the author/funder. All rights reserved. No reuse allowed without permission.

Figure 3

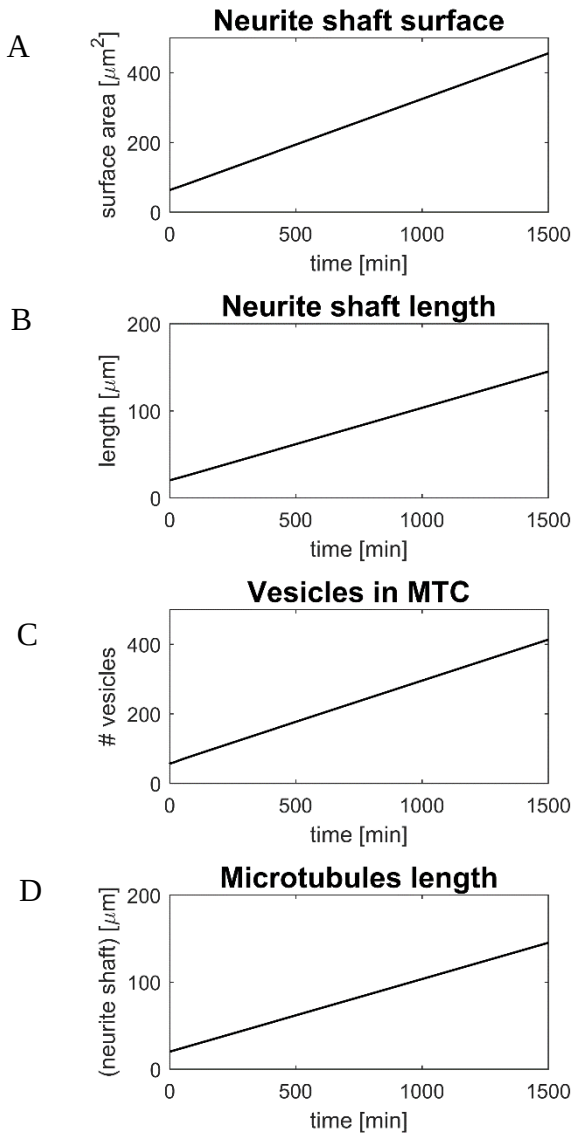

Figure 3: Simulation of vesicular transport and microtubule growth during neurite outgrowth. We identified a set of parameters and protein concentrations that allows neurite outgrowth with a velocity of 5 µm/h. **(A)** Outgrowth depends on the continuous addition of membrane to the neurite shaft **(B)** that allows neurite shaft length increase linearly. **(C)** The vesicles in the microtubule transport compartment that fills out the interior of the neurite shaft grows in parallel to the neurite shaft, causing an increase in both moving and stationary vesicles. (D) The microtubule scaffold grows with the same velocity.

bioRxiv preprint doi: https://doi.org/10.1101/153569; this version posted June 23, 2017. The copyright holder for this preprint (which was not certified by peer review) is the author/funder. All rights reserved. No reuse allowed without permission.

Figure 4A

Calculation of membrane fluxes and initial amounts

Characterization of different membrane vesicle types based on final destination of membrane vesicles
Calculation of fluxes of membranes of each type

⇦ NOG velocity, Rate of membrane cycling, Size and fraction of actively transported anterograde and retrograde vesicles in MTC, TGN and GC sizes, initial neurite length → initial MTC length

⇩

Calculation of initial and final forward and backward rate of membrane vesicle transport

⇦ Recruitment factor 1 at TGN, recruitment factor 2 at GC

⇩

Membrane synthesis at TGN
Budding rates of vesicles at TGN and GC
Initial vesicles in each cytoplasmic compartment

Calculation of v-SNARE fluxes

Calculation of v-SNARE V in GC cytoplasm
Calculation of v-SNARE U in CB cytoplasm

⇦ t-SNARE Y at GC, tethering rate for V and Y SNARE-complex formation at GC, t-SNARE X at TGN, tethering rate for U and X SNARE-complex formation at TGN, fraction of moving (i.e. fusing) vesicles in GC cytoplasm and CB cytoplasm

⇩

Calculation of initial and final forward and backward fluxes for SNARE V and SNARE U

⇩

Calculation of SNARE U and V at GC and TGN

Calculation of motor protein receptor fluxes

Calculation of kinesin receptors for anterograde vesicles in MTC and dynein receptors for retrograde vesicles in MTC

⇦ Fraction of actively transported anterograde and retrograde vesicles in MTC

⇩

Calculation of initial and final forward and backward fluxes of kinesin and dynein receptors

Calculation of t-SNARE and recruitment factor fluxes

Calculation of protein production rates at TGN

Calculate protein production rates at TGN to compensate for membrane proteins that are not trapped in MTC

Calculation of microtubule growth behavior

Calculation of nucleation and conversion rates

⇦ NOG velocity, effective tubulin concentration, length of dynamic MTs, nucleation rate

bioRxiv preprint doi: https://doi.org/10.1101/153569; this version posted June 23, 2017. The copyright holder for this preprint (which was not certified by peer review) is the author/funder. All rights reserved. No reuse allowed without permission.

Figure 4B

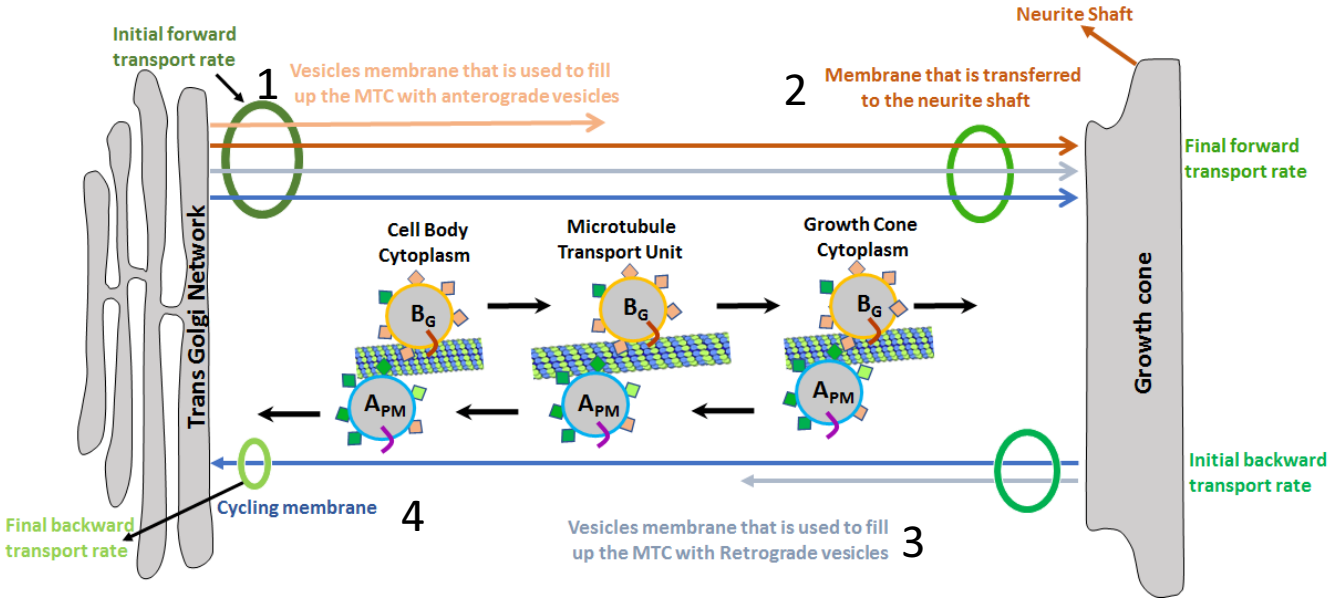

Figure 4C

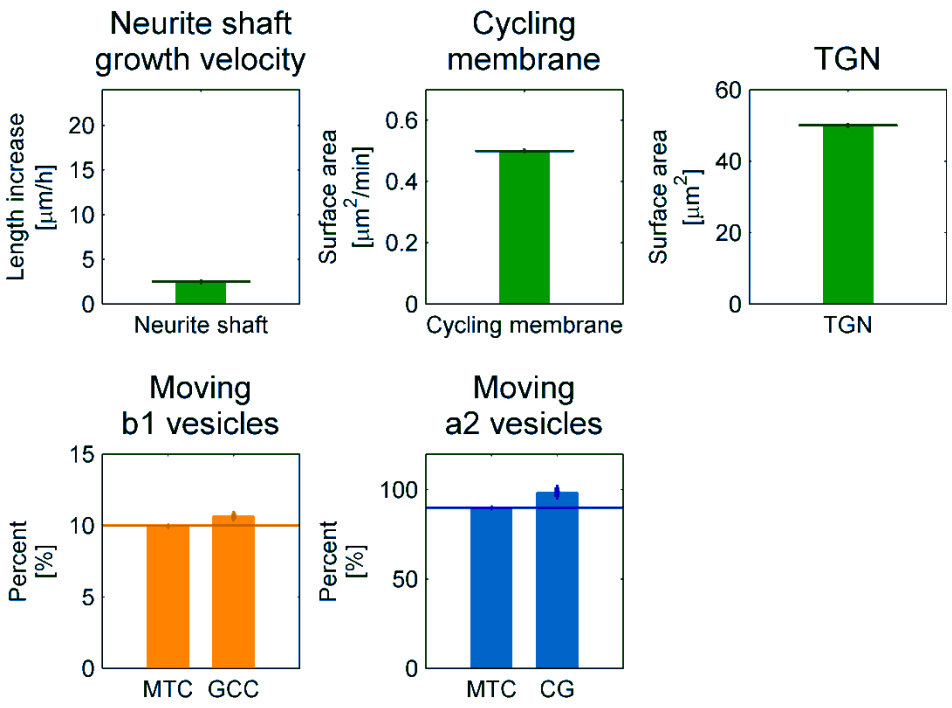

bioRxiv preprint doi: https://doi.org/10.1101/153569; this version posted June 23, 2017. The copyright holder for this preprint (which was not certified by peer review) is the author/funder. All rights reserved. No reuse allowed without permission.

Figure 4D

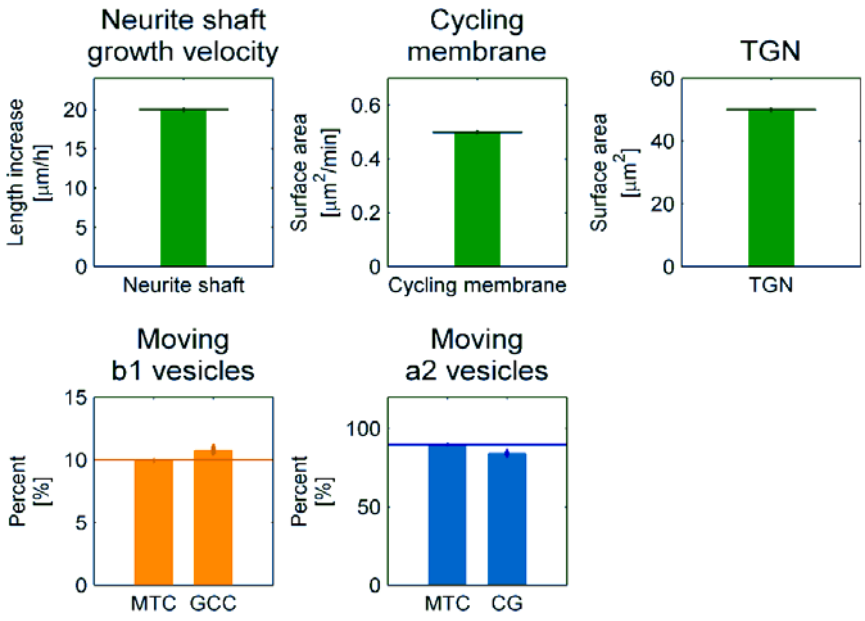

Figure 4: Development of analytical solution algorithms for the identification of sets of initial protein amounts and parameter that allow NOG at a fixed velocity of choice. For a systematic analysis of the dynamical model we generated an algorithm that predicts sets of parameters and protein amounts in the different compartments that enable neurite outgrowth at a fixed velocity of choice within the constraints on SCP dynamics that result in a steady growth velocity. **(A)** The algorithm calculates dependent parameters and initial amounts (right-side) based on specified parameters and initial amounts (right side). See main text for details. **(B)** The membrane vesicle that buds from the TGN can be separated into 4 different membrane vesicle types based on the final destination. The arrows refer to the different membrane vesicle types and point at the final destination. Orange arrows label membrane vesicle types that are only transported by anterograde movement, while blue arrows label membrane vesicle types that are transported by both anterograde and retrograde movement. Green circles summarize those membrane vesicle types that are combined to obtain initial and final forward and back transport rates. See main text for details. (**C-D)**We used protein amounts and parameter that were predicted for 5 different tethering rates of the GC membrane vesicles and 9 different NOG velocities (see dots in fig 5A) as initial protein concentrations and parameter sets and simulated neurite outgrowth over a time period of 5000 minutes(~3.5 days). Every 1000min we obtained the numerical results and averaged them for each velocity (**C**: 2.5 µm/h, **D**: 20 µm/h). Bars indicate steady state levels of the selected target outputs, horizontal lines the specified model constraint for that output. Vertical lines indicate standard deviations. See supplementary figure 4 for all results and initial specified values.

bioRxiv preprint doi: https://doi.org/10.1101/153569; this version posted June 23, 2017. The copyright holder for this preprint (which was not certified by peer review) is the author/funder. All rights reserved. No reuse allowed without permission.

Figure 5

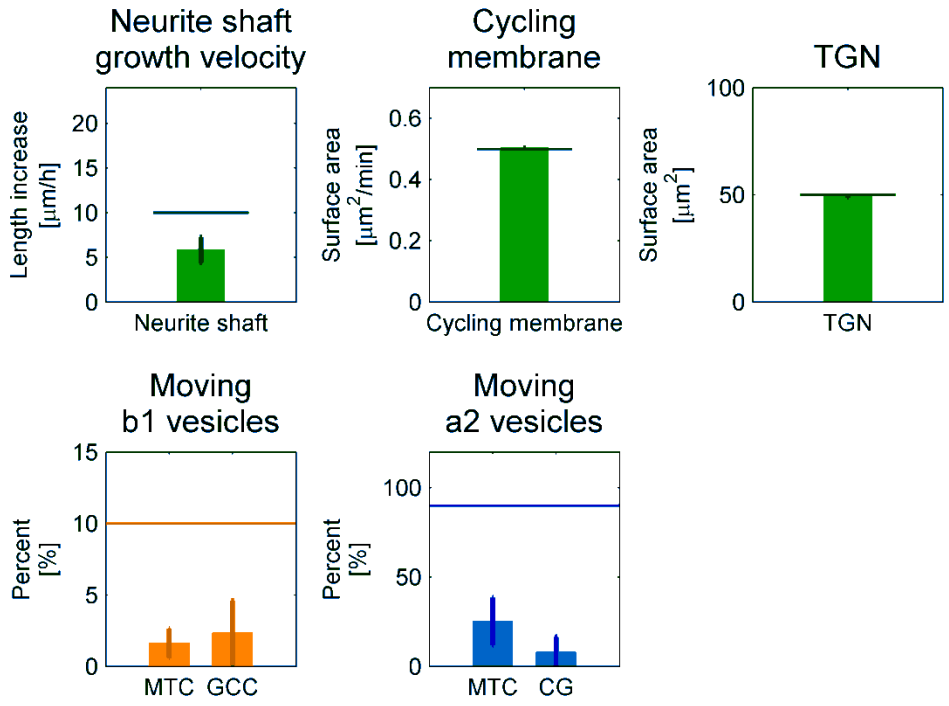

Figure 5: Un-coordinated SCP activities decrease ability for NOG and inappropriate distribution of components in compartments. Initial protein amounts and parameters that were predicted based on an anticipated NOG velocity of 5 µm/h and 10 µm/h and 5 different tethering rates as described in figure 4 were combined to simulate NOG when the SCPs involved in membrane synthesis and delivery and gene protein production are uncoordinated. Initial protein amounts, parameters and membrane production rate were taken from the predictions based on a rate of 10 µm/h, while protein production rates were taken from the predictions For NOG with a velocity of 5 µm/h. Numerical simulations yielded results as obtained as described in Figure 4, Horizontal lines indicate the defined model constraints. The example demonstrates that NOG without complications depends on the highly coordinated activities of the individual SCPs.

bioRxiv preprint doi: https://doi.org/10.1101/153569; this version posted June 23, 2017. The copyright holder for this preprint (which was not certified by peer review) is the author/funder. All rights reserved. No reuse allowed without permission.

Figure 6

Vesicle tethering and fusion

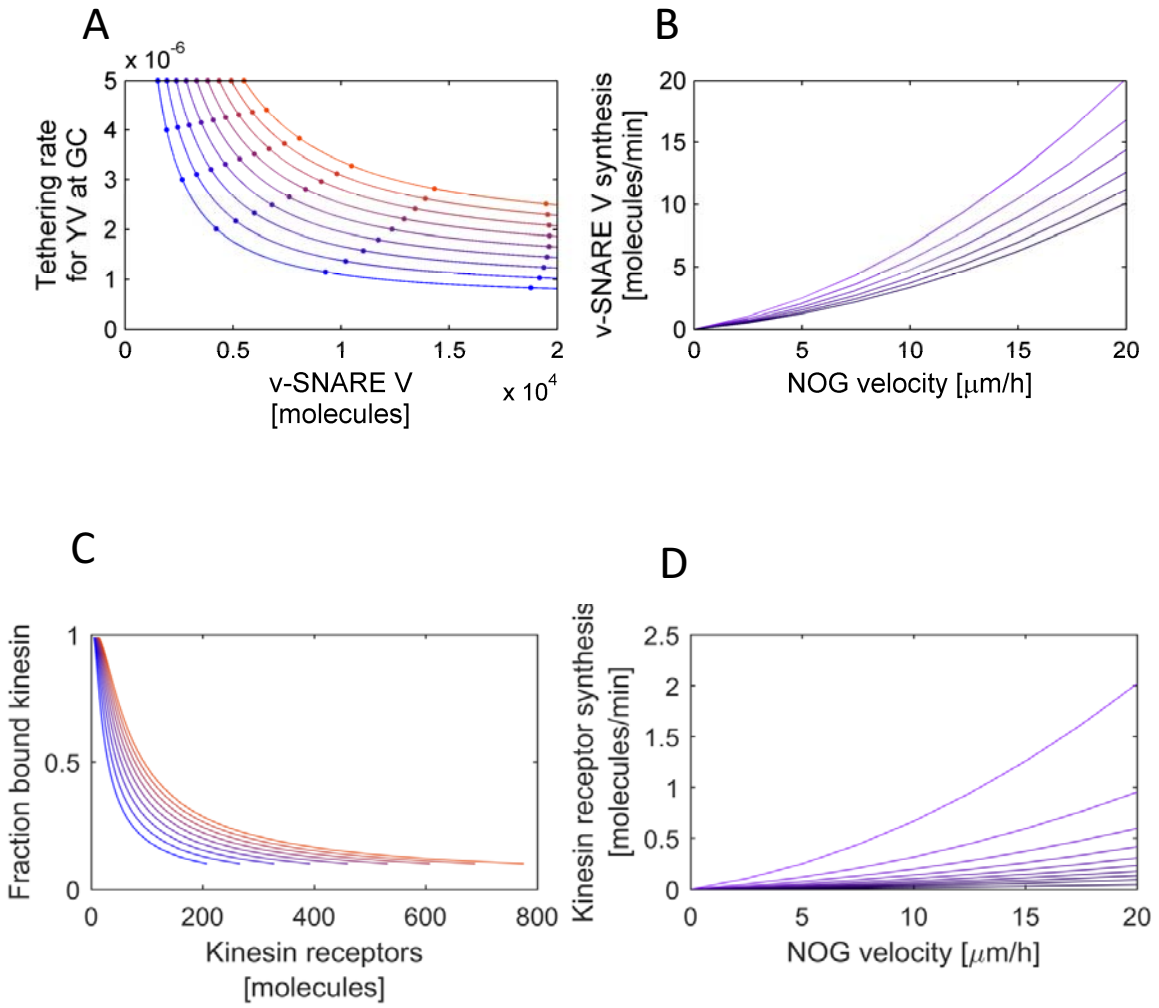

Figure 6: Complementary SCPs need to be coordinated for neurite outgrowth. To analyze the relationship between complementary SCPs we generated an analytical solution for the prediction of steady state dynamics that enable neurite outgrowth for a specified velocity. **(A)** Vesicle fusion with the growth cone membrane depends on the coordinated activity of vesicle tethering and SNARE complex formation. Multiple combinations of parameters for vesicle tethering at the GC membrane and SNARE complex formation allow neurite outgrowth for a specified velocity with the requirement that 10% of the vesicles in the growth cone should fuse with the plasma membrane. We assumed a tethering rate at the TGN of $8x10^{-6}$/molecule. The relationship between vesicle tethering activity and total amount of v-SNARE V is shown for the velocities 0, 2.5, 5, 7.5, 10, 12.5, 15, 17.5 and 20 (from blue to orange) µm/h. v-SNARE amounts refer to the amounts at the beginning of neurite outgrowth, i.e. before the MTC compartment

bioRxiv preprint doi: https://doi.org/10.1101/153569; this version posted June 23, 2017. The copyright holder for this preprint (which was not certified by peer review) is the author/funder. All rights reserved. No reuse allowed without permission.

increases. Dots mark those constellations that were used to compare the analytical prediction with the numerical outcome (Fig 4C). **(B)** With an increase in the MTC, more v-SNAREs need to be produced to compensate for the v-SNAREs that are 'consumed' by the MTC. The production rates for SNARE V increases with decreasing tethering rate (from dark violet to bright violet: $5x10^{-6}$, $4.5x10^{-6}$,$4x10^{-6}$, $3.5x10^{-6}$, $3x10^{-6}$, $2.5x10^{-6}$) and with increasing velocity. **(C)** The fraction of bound kinesin and the amount of kinesin receptors are in a similar hyperbolic relationship at the beginning of neurite outgrowth. The combined activities of both components ensure that 90% of the vesicles in the MTC are stationary parts of the MTC membrane reservoir. Velocities are the same as in A. **(D)** A decrease in the fraction of bound kinesin due to change in dissociation constant (from dark violet to bright violet: 1, 0.9, 0.8, 0.7, 0.6, 0.5, 0.4, 0.3, 0.2, 0.1) increases the needed kinesin receptor production rate. Similarly, for the production rate for SNARE V, the needed production rates for kinesin receptors increases over proportionally with the outgrowth velocity.

bioRxiv preprint doi: https://doi.org/10.1101/153569; this version posted June 23, 2017. The copyright holder for this preprint (which was not certified by peer review) is the author/funder. All rights reserved. No reuse allowed without permission.

Figure 7

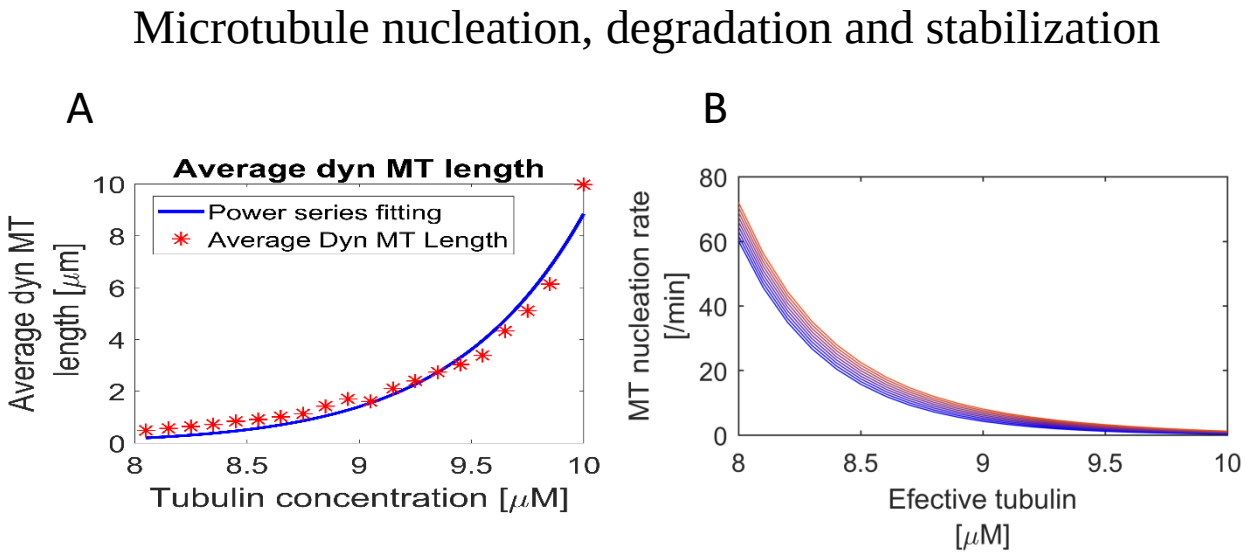

Figure 7: Tubulin concentration dependent average dynamic MT length and nucleation rate.(A) In a pre-simulation using a published model (Margolin et al. 2012) we determined the dependence of the average length of the dynamic microtubules on effective tubulin concentration. The average length increases exponentially with the tubulin concentration. **(B)** The same microtubule scaffold growth for the velocities 0, 2.5, 5, 7.5, 10, 12.5, 15, 17.5 and 20 (from blue to orange) in µm/h can be achieved via indicated combinations of MT nucleation rates and effective tubulin concentrations. Based on the prediction that the length of the dynamic MTs exponentially increases with the effective tubulin concentration, our simulations predict that with higher velocities, less additional effective tubulin is necessary to further increase the microtubule growth velocity.

Table 1: Reactions for the vesicle transport model

Reaction #	Description	Compartment	Reaction	Parameters	Molecules
1.	Membrane lipid production	TGN	$k_{\text{membrane production}}$	k_{MP}	
2.	Anterograde vesicle budding at Golgi	TGN➔CBC	$f_1 = w_G^B * S_G * R_{1_G}$	w_G^B	R_{1_G}
3.	Saturation function for carrying V-SNAREs to vesicles that bud from the TGN mediated by coat B	Anterograde Vesicles	$\phi_{sv}^{B_G} = S^{\psi} \times \left(\frac{\frac{sv_G}{k_{sx}^B}}{1 + \frac{sx_G}{k_{sx}^B} + \frac{su_G}{k_{su}^B} + \frac{sy_G}{k_{sy}^B} + \frac{sv_G}{k_{sv}^B}} \right)$	k_{sx}^B, k_{su}^B k_{sy}^B, k_{sv}^B S^{ψ}	sx_G, su_G sy_G, sv_G
4.	Saturation function for carrying kin_G to vesicles that bud from the TGN mediated by coat B	Anterograde Vesicles	$\phi_{kin}^{B_G} = M^{\psi} \times \left(\frac{\frac{kin_G}{k_{kin}^B}}{1 + \frac{kin_G}{k_{kin}^B}} \right)$	k_{kin}^B M^{ψ}	kin_G
5.	Saturation function for carrying r_{1_G} to vesicles that bud from the TGN mediated by coat B	Anterograde Vesicles	$\phi_{r_1}^{A_G} = R^{\psi} \times \left(\frac{\frac{r_{1_G}}{k_{r_1}^B}}{1 + \frac{r_{1_G}}{k_{r_1}^B}} \right)$	$k_{r_1}^B$ R^{ψ}	r_{1_G}
6.	Anterograde vesicle dynamics in CBC compartment	CBC➔MTC	$(a)\quad \#k_{CBC}^{B_G} = \frac{kin_{CBC}^{B_G}}{\#N_{CBC}^{B_G}}$, $(b)\quad fN_{CBC}^{B_G} = 1 - \left(1 - f_{CBC}^{kin}\right)^{\#k_{CBC}^{B_G}}$, $(c)\quad f_2 = \frac{N_{CBC}^{B_G}}{T_{CBC}} * fN_{CBC}^{B_G}, \quad T_{CBC} = \frac{L_{CBC}}{v_k}$	v_k, f_{CBC}^{kin}, $\#k_{CBC}^{B_G}$	$kin_{CBC}^{B_G}$
7.	Anterograde vesicle transport in cytoplasmic compartment, shown for example MTC	MTC➔ GCC	$(a)\quad \#k_{MTC}^{B_G} = \frac{kin_{MTC}^{B_G}}{\#N_{MTC}^{B_G}}$, $(b)\quad fN_{MTC}^{B_G} = 1 - \left(1 - f_{MTC}^{kin}\right)^{\#k_{MTC}^{B_G}}$, $(c)\quad f_2 = \frac{N_{MTC}^{B_G}}{T_{MTC}} * fN_{CBC}^{B_G}, \quad T_{MTC} = \frac{L_{MTC}}{v_k}$	v_k, f_{MTC}^{kin} $\#k_{MTC}^{B_G}$	$kin_{MTC}^{B_G}$
8.	Vesicle fusion with target membrane, shown for example of anterograde vesicles with growth cone membrane	GCC➔ GC	$f_4 = \left(\begin{array}{l} \kappa_{XU} \times SX_{GCC}^{B_G} \times SU_{PM} \\ + \kappa_{XU} \times SU_{GCC}^{B_G} \times SX_{PM} \\ + \kappa_{YV} \times SY_{GCC}^{B_G} \times SV_{PM} \\ + \kappa_{YV} \times SV_{GCC}^{B_G} \times SY_{PM} \end{array} \right) * \frac{\left(1 - fN_{GCC}^{B_G}\right) * S_{AVSA}}{R_{SCPVF}}$	κ_{XU}, κ_{YV}, $fN_{GCC}^{B_G}$	$SX_{GCC}^{B_G}$, SU_{PM}, $SU_{GCC}^{B_G}$, SX_{PM}, $SY_{GCC}^{B_G}$, SV_{PM}, $SV_{GCC}^{B_G}$, SY_{PM}

bioRxiv preprint doi: https://doi.org/10.1101/153569; this version posted June 23, 2017. The copyright holder for this preprint (which was not certified by peer review) is the author/funder. All rights reserved. No reuse allowed without permission.

bioRxiv preprint doi: https://doi.org/10.1101/153569; this version posted June 23, 2017. The copyright holder for this preprint (which was not certified by peer review) is the author/funder. All rights reserved. No reuse allowed without permission.

Table 2: Dissociation constants of membrane proteins for interactions with the coat proteins Dissociation constants were selected to ensure preferred binding of proteins that are involved in anterograde transport to coat B and proteins that are involved in retrograde transport to coat A. High dissociation constants for stationary proteins for those coat proteins that would incorporate them into vesicles involved in back transport were selected to ensure that these proteins stay at their anticipated organelle. Orange: Proteins involved in anterograde movement, Blue: Proteins involved in retrograde movement, *Italics*: Proteins that cycle between the TGN and GC, Standard fonts: stationary molecules.

Dissociation constants for interactions with Coat B	
SNAREs	***v-SNARE V*** *($K_d = 1$)*, **t-SNARE Y** *($K_d = 1$)* < ***v-SNARE U*** *($K_d = 100$)* > **t-SNARE X** *($K_d = 10000$)*
Motor protein receptors	***kinesin receptor*** *($K_d = 0.1$)* < ***dynein receptor*** *($K_d = 10$)*
Recruitment factors	**recruitment factor 1** *($K_d = 1$)* < **recruitment factor 2** *($K_d = 100000$)*
Dissociation constants for interactions with Coat A	
SNAREs	***v-SNARE U*** *($K_d = 1$)*, **t-SNARE X** *($K_d = 1$)* < ***v-SNARE V*** *($K_d = 100$)* > **t-SNARE Y** *($K_d = 10000$)*
Motor protein receptors	***dynein receptor*** *($K_d = 0.1$)* < ***kinesin receptor*** *($K_d = 10$)*
Recruitment factors	**recruitment factor 2** *($K_d = 1$)* < **recruitment factor 1** *($K_d = 100000$)*

bioRxiv preprint doi: https://doi.org/10.1101/153569; this version posted June 23, 2017. The copyright holder for this preprint (which was not certified by peer review) is the author/funder. All rights reserved. No reuse allowed without permission.

Table 3 Reactions for Microtubule Bundle Growth

Reaction #	Description	Reaction	Parameters	Molecules
9.	Nucleation of dynamic microtubules	$\frac{d\ MT_{Nu}}{dt} = \beta_1$	β_1	
10.	Average dynamic MT length	$L_1 = \theta_1 \times \theta_2$	θ_1, θ_2	$effective\ tubulin$
11.	Degradation rate of dynamic microtubules	$\beta_2 = a \times [effective\ tubulin]^b$	a, b	$effective\ tubulin$
12.	Change in number of dynamic MTs	$\frac{d\ N_1}{dt} = \beta_1 - \gamma \times N_1 - \beta_2 \times N_1$	β_1, γ, β_2	
13.	Increase in length of stable MTs	$\frac{d\ L_{stbl}}{dt} = \gamma \times L_{dyn}$	γ, L_{dyn}	
14.	Combined length of dynamic MTs	$L_{dyn} = L_1 \times N_1$	L_1, N_1	
15.	Microtubule scaffold length	$L_{MTB} = \frac{L_{dyn} + L_{stbl}}{N_2}$	N_2	
16.	Neurite Length	$L = \frac{s_3}{2 \times \pi \times r_{neurite}}$	$r_{neurite}$	

bioRxiv preprint doi: https://doi.org/10.1101/153569; this version posted June 23, 2017. The copyright holder for this preprint (which was not certified by peer review) is the author/funder. All rights reserved. No reuse allowed without permission.

Table 4: Percentages of microtubule (MT) bound/unbound motor protein in the different compartments: A high fraction of MT-bound kinesin in the cell body cytoplasm ensures that vesicles are immediately transported forward after budding from the TGN. A low percentage of bound kinesin in the MTC causes about 90% of the anterograde vesicles in the MTC to be stationary and constitute a membrane mobilization reservoir that can be recruited upon demand. No kinesin is bound to the MT in the GC cytoplasm, so that all anterograde vesicles are available for fusion with the GC membrane. The percentages of MT-bound dynein in the GC and CB cytoplasm were selected for the same reason. Since we do not assume that there is a membrane reservoir for retrograde vesicle, we selected a high percentage of bound dynein in the MTC.

Percentage of motor Bound to microtubules	Cell body cytoplasm	Motor transport unit	Growth cone cytoplasm
Percentage of kinesin bound/unbound	95 /5	8 /92	0 /100
Percentage of Dynein bound/unbound	0/100	84/ 16	95 /5